

Bendik Bartnes

Compressor Fouling

Master's thesis in Mechanical Engineering

Supervisor: Lars Eirik Bakken

July 2020

Bendik Bartnes

Compressor Fouling

Master's thesis in Mechanical Engineering
Supervisor: Lars Eirik Bakken
July 2020

Norwegian University of Science and Technology
Faculty of Engineering
Department of Energy and Process Engineering



Abstract

For oil and gas companies to be competitive in today's market, increased efficiency of production and improved field recovery are of great importance. Utilizing innovative technologies such as subsea wet gas compression can be one way of achieving this. Advantages of this technology includes, enhanced recovery rates, reduced investment cost due to fewer components and reduced size of system. Despite the advantages, wet gas compression is extremely complex and is still a relatively new technology. This results in the degradation mechanisms associated with wet gas compression not being fully understood. An important deteriorating mechanism for compressor operation is fouling, which for dry gas compression have shown to reduce the polytropic efficiency, head and pressure ratio.

The impact of diffuser fouling on the compressor performance for both dry and wet gas compression has been experimentally tested at the NTNU compressor lab. Fouling replication with the use of texturized paint has been documented. Its durability towards wet gas flow, particle production, impact on liquid flow regime, and application and removal process have been covered. A total of 11 coats of texturized paint were successfully applied to the hub side of the diffuser section to obtain a material build up representative of industry findings.

The obtained test results clearly document a reduction in polytropic efficiency, polytropic head and pressure ratio for fouled conditions with the reduction being most severe at high flow rates. However, an increase in compressor performance compared to their respective clean tests was observed for the two lowest GMFs at low flow rates. The best efficiency point was seen to be shifted towards lower flow rates and a reduction in the maximum throughput was observed for fouled conditions for all GMFs compared to their respective clean tests. Fouling of the diffuser section was also observed to enhance both the head rise to surge and pressure ratio rise to surge for all tested GMFs, with the increase being greatest for lower GMFs.

Sammendrag

For at olje- og gasselskaper skal kunne være konkurransedyktige i dagens marked, er økt effektivitet i produksjonen og forbedret feltutvinning av stor betydning. En måte å oppnå dette på kan være å bruke nyskapende teknologi som subsea-våtgasskompresjon. Fordelelene med denne teknologien inkluderer forbedrede utvinningsgrad, reduserte investeringskostnader grunnet færre komponenter og redusert størrelse på systemet. Til tross for fordelene er flerfasekompresjon ekstremt komplisert og er fremdeles en relativt ny teknologi. Dette resulterer i at degraderingsmekanismene assosiert med våtgasskompresjon ikke er fullstendig forstått. En viktig degraderingsmekanisme for kompressordrift er beleggdannelse, som for tørrgasskompresjon har vist å redusere polytropisk effektivitet, løftehøyde og trykkforhold.

Effekten av beleggdannelse i diffusersesksjonen på kompressorens ytelse for både tørr- og våt-gasskompresjon er eksperimentelt testet ved kompressorlabben på NTNU. Beleggdannelse har blitt etterlignet ved hjelp av metallmaling tilsatt pleksiglasspartikler. Beleggets holdbarhet mot våtgasstrømning, partikkelproduksjon, innvirkning på strømningsregimet til væsken, og påførings- og fjerningsprosess har blitt dekket. Totalt 11 strøk med teksturmaling ble vellykket påført den bakre diffuserveggen for å oppnå en beleggtykkelse representativ funn fra industrien.

De oppnådde resultatene dokumenterer tydelig en reduksjon i polytropisk effektivitet, polytropisk løftehøyde og trykkforhold for beleggtestene, hvor reduksjonen var observerer mest markant for høye volumstrømmer. Det ble imidlertid observer, for de to laveste GMFene, en økning i kompressorytelsen sammenlignet med deres respektive rene tester for lave strømnings-rater. Det ble observert en forskyvning av det beste effektivitetspunktet mot lavere volumstrømmer, samt en reduksjon i den maksimale gjennomstrømningsraten for alle GMFene når en gikk fra ren til belagt diffusersesksjon. Beleggdannelse i diffusjon-sesksjonen ble også observert å øke både "head rise to surge" og "pressure ratio rise to surge" for alle testede GMFer. Økningen ble observert til å være størst for lavere GMFer.

Preface

This master's thesis, titled "Compressor Fouling" concludes my Master of Science program in Mechanical Engineering at the Norwegian University of Science and Technology (NTNU). The work has been conducted during the spring semester of 2020 and equates a total of 30 ECTS credits.

I would like to thank and extend my gratitude towards my supervisor Lars E. Bakken and my co-supervisors Erik Langørgen, Øyvind Hundseid and Tor Bjørge for their support and guidance during the master's thesis.

I would also like to thank my fellow students working at the compressor test facility for being great theoretical sparring partners and a source of helpful discussions.

Trondheim, July 4th, 2020

Bendik Bartnes

Table of Contents

Abstract	i
Sammendrag	iii
Preface	v
Table of Contents	x
List of Tables	xi
List of Figures	xvi
Nomenclature	xvii
1 Introduction	1
1.1 Background	1
1.2 Scope of Thesis	2
1.3 Limitations of Scope	3
1.4 Information Retrieval	3
1.5 Report Structure	4

2	Compressor Fundamentals	5
2.1	Operational Principles	5
2.1.1	Theoretical, Ideal and Actual Head	6
2.1.2	Compressor Maps and Characteristics	7
2.1.3	Head Rise to Surge	8
2.2	Compressor Losses	9
2.2.1	Skin Friction Losses	9
2.2.2	Blockage Losses	10
2.2.3	Incidence Losses	10
2.3	Dry Gas Polytropic Performance	11
2.4	Liquid Impact	12
2.4.1	Energy Transfer	12
2.4.2	Basic Wet Gas Parameters	12
2.4.3	Multiphase Effects on Compressor	14
2.5	Wet Gas Polytropic Performance	15
2.6	Summary	17
3	Compressor Fouling	19
3.1	Fouling Mechanisms	19
3.2	Entrainment	20
3.3	Sticking Mechanisms	22
3.4	Effect of Compressor Fouling	23
3.4.1	Inducer	23
3.4.2	Impeller	25
3.4.3	Diffuser	26
3.5	Fouling Correction Models	27

3.6	Summary	30
4	Fouling replication	31
4.1	Attributes of Fouling Material	32
4.2	Reviewed Materials	33
4.3	Metallic Texturized Paint	34
4.3.1	Durability	34
4.3.2	Plexiglas Particles	34
4.4	Diffuser Fouling Replication	36
4.5	Application and Removal Procedure	36
4.6	Summary	39
5	Experimental Campaign	41
5.1	The NTNU Wet Gas Compressor Test Facility	41
5.2	Objectives	44
5.3	Test Campaign	44
5.3.1	Logging of Operational Parameters	44
5.3.2	Fouled Diffuser Test	45
5.3.3	Unfouled Baseline Tests	46
5.3.4	Test Procedure	46
5.3.5	Data Processing	47
5.3.6	Experimental Uncertainties	48
5.4	Summary	50
6	Results and Discussion	51
6.1	Performance Characteristics	51
6.1.1	Clean Baseline Performance	52

6.1.2	Effect of Fouling on Polytropic Head	54
6.1.3	Reduction in Polytropic Head Due to Fouling	55
6.1.4	Fouling Impact on Pressure Ratio	56
6.1.5	Fouling Effect on Polytropic Efficiency	58
6.1.6	Deviation in Polytropic Efficiency	60
6.1.7	Fouling Impact on Flow Throughput	61
6.1.8	Fouling Impact on Surge Margin	61
6.2	Coating Experience	62
6.2.1	Wet and Dry Gas Resistance	62
6.2.2	Fouling Influence on Diffuser Flow Pattern	63
7	Conclusion and Further Works	65
7.1	Conclusion	65
7.2	Further Works	66
	Bibliography	66
A	Schultz Method	I
B	HYSYS Model	III
C	Risk Matrix	V

List of Tables

5.1	Main dimensions and operating ranges of NTNU wet gas compressor setup	43
5.2	Operational test points at 9000 RPM with corresponding discharge valve openings.	45
5.3	Test matrix for the fouled diffuser tests for dry and wet gas compression. .	46
5.4	Test matrix for the fouled diffuser tests for dry and wet gas compression. .	46

List of Figures

1.1	Gullfaks C wet gas compressor.	2
2.1	Overview of backswept centrifugal compressor with corresponding velocity triangles.	6
2.2	Graphical representation of the theoretical, ideal and actual head with corresponding losses for backswept centrifugal compressor.	7
2.3	Centrifugal compressor map where the the operational domain, surge and choked operations are visualized for a compressor curve.	8
2.4	Graphical representation of the polytropic compression path.	11
2.5	Change in impeller outlet velocity triangle resulting from liquid introduction.	13
2.6	Compressor characteristic curves for different GMFs ranging from 1 to 0.6 with water and air as the operating fluids	16
3.1	Representation of the governing compressor fouling entrainment mechanisms.	20
3.2	Close up of impeller and diffuser hub side of a multistage hydrocarbon compressor previously operating at Åsgård.	23
3.3	Dry and wet gas normalized polytropic efficiency plotted against normalized total volume flow rate for both clean and fouled conditions.	24

3.4	Dry and wet gas normalized polytropic heap plotted against normalized total volume flow rate for both clean and fouled conditions.	24
3.5	Normalized pressure ratio for GMF 0.975 and 0.90 plotted against normalized total volume flow rate for both clean and fouled conditions.	25
3.6	The relative change in polytropic efficiency and head when going from clean to fouled condition for GMF 1, 0.975 and 0.90.	25
3.7	A visual representation of friction correction method.	29
3.8	A visual representation of the application domain for the Reynolds correction method.	29
4.1	Fouled last stage diffuser hub of retired multistage compressor previously operating at Åsgard - now located at the NTNU wet gas compression facility.	31
4.2	Deposits collected from different components of a hydrocarbon compressor at K-lab.	32
4.3	Emery cloth fouling replication before and prior to power washer stream test.	33
4.4	Obtained results from durability tests for the Hammerite and Bengalack coated test plates.	35
4.5	Sizes of the Plexiglas particles with with a caliper as reference. The unprocessed shavings is seen to the right, the first size reduction in the middle and the final reduction step to the left.	35
4.6	A visual of the hub side of the diffuser prior and after the fouling replication procedure in addition to a cross sectional view of the applied coating.	37
4.7	Visualization of the extended coating obtained to prevent flow digging under the fouling replica.	37
4.8	Surface finish of of the final coating layer before and after roughening with emery cloth.	38
4.9	Diffuser section during and after removal of texturized paint.	38
5.1	NTNU wet gas compressor displaying the liquid injection module.	42
5.2	Nozzle layout of water injection module.	42

5.3	Test rig P&ID with corresponding test rig instrumentation and accuracy . . .	43
6.1	Normalized polytropic head curves for the tested GMFs at clean conditions.	52
6.2	Normalized pressure ratio curves for the tested GMFs at clean conditions.	53
6.3	Normalized polytropic efficiency for tested GMFs at clean conditions. . . .	53
6.4	Normalized polytropic head curves for the clean and fouled dry gas compression tests.	54
6.5	Normalized polytropic head curves for clean and fouled conditions for GMF 0.99 and 0.975.	55
6.6	Normalized polytropic head curves for clean and fouled conditions for GMF 0.90 and 0.80.	56
6.7	The relative reduction in polytropic head when going from clean to fouled scenarios for the tested GMFs.	56
6.8	Normalized pressure ratio curves the for clean and fouled dry gas compression tests.	57
6.9	Normalized pressure ratio curves for clean and fouled conditions for GMF 0.99 and 0.975.	57
6.10	Normalized pressure ratio curves for clean and fouled conditions for GMF 0.90 and 0.80.	58
6.11	Normalized polytropic efficiency curves the for clean and fouled dry gas compression tests.	59
6.12	Normalized polytropic efficiency curves for clean and fouled conditions for GMF 0.99 and 0.975.	59
6.13	Normalized pressure ratio curves for clean and fouled conditions for GMF 0.90 and 0.80.	60
6.14	The relative reduction in polytropic efficiency when going from clean to fouled scenarios for the tested GMFs.	61
6.15	State of the coating before and after the conducted experimental campaign and 5 hour maximum load test.	63
6.16	Power washer water jet impacting a clean aluminum test plate.	64
6.17	Power washer water jet impacting a fouled aluminum test plate.	64

B.1 HYSYS steady state model used for polytropic head and efficiency calculations.	III
--	-----

Nomenclature

Latin symbols

Symbol	Description	Unit
c	Absolute velocity	m/s
d	Diameter	m
e	Peak-to-valley surface roughness	m
f	Head correction factor	[-]
h	Specific enthalpy	kJ/kg
H	Head	kJ/kg
k	Specific heat ratio	[-]
L	Blade mean streamline meridional length	m
\dot{m}	Mass flow rate	kg/s
MW	Molecular weight	kg/mol
n	Polytropic exponent	[-]
p	Pressure	Pa
P	Power	W
Q	Volume flow rate	m^3/s
R_0	Universal gas constant	$J/(mol \cdot K)$
Re	Reynolds number	[-]
s	Specific entropy	J/K
Stk	Stokes Number	[-]
T	Temperature	K
U	Impeller tip speed	m/s
v	Specific volume	m^3/kg
w	Relative velocity	m/s
\bar{w}	Quadratic mean relative velocity	m/s
X	Compressibility function	[-]
Y	Compressibility function	[-]
Z	Compressibility function	[-]

Greek Symbols

Symbol	Description	Unit
α	Gas volume fraction	[-]

continued on next page

Symbol	Description	Unit
α_{Re}	Fraction of Reynold dependent losses	[-]
β	Relative flow angle	°
γ	Gas mass fraction	[-]
δ	Density ratio	[-]
Δq	Adiabatic head loss coefficient	[-]
η	Efficiency	[-]
κ	Isentropic exponent	[-]
λ	Friction factor	[-]
μ	Dynamic viscosity	$kg/(s \cdot m)$
ν	Kinematic viscosity	m^2/s
ρ	Density	kg/m^3
τ	Fluid response time	s
ϕ	Flow coefficient	[-]
ψ	Polytropic head coefficient	[-]

Subscripts

Index	Description
1	Impeller inlet
2	Impeller exit
3	Diffuser exit
b	Diffuser width
<i>clean</i>	Clean condition
<i>cr</i>	Critical conditions
<i>fouled</i>	Fouled condition
g	Gas
h	Hydraulic
<i>inc</i>	Incidence
l	Liquid
<i>mid</i>	Midpoint between point 1 and 2
<i>mp</i>	Multiphase
p	Polytropic
<i>par</i>	Particle
r	Radial component
s	Isentropic
<i>sf</i>	Skin friction
<i>sp</i>	Specified condition
t	Theoretical
T	Temperature
<i>test</i>	Test condition

continued on next page

Index	Description
v	Volume
x	Axial component
θ	Tangential components

Superscripts

Index	Description
'	Geometric

Abbreviations

Abbreviation	Description
3D	Three-Dimensional
ASME	The American Society of Mechanical Engineers
BEP	Best Efficiency Point
CAPEX	Capital Expenditure
CFD	Computational Fluid Dynamics
GMF	Gas Mass Fraction
GVF	Gas Volume Fraction
ISO	International Organization for Standardization
MEG	Monoethylene glycol
NTNU	Norwegian University of Science and Thechnology
OP	Operational Point
P&ID	Piping and instrumentation diagram
PTC	Performance Test Code
RPM	Rotations Per Minute
SSS	Semi Steady State

Introduction

1.1 Background

As most of the larger oil and gas fields have already been explored, new big discoveries are rare. The oil and gas industry has thus devoted more attention to marginal field development and extended tail end production. Subsea wet gas compression is a newly proven and innovative technology that enables the pressurization of a gas-liquid-mixture, with gas volume fractions (GVF) typically in the range of 95% - 100%. It represented a breakthrough in compressor operation as it enables the compression of unprocessed well streams. Subsea wet gas compression allows for a CAPEX reduction due to reduced component requirements for the subsea module. The technology will reduce the load on topside facilities in addition to decrease the spatial impact on the seabed as a result of smaller subsea units. Other incentives for adopting subsea wet gas compression include its capability of enhanced recovery rates through pressure boosting and cost efficiently increase the tieback distance of subsea gas fields. Equinor estimates their utilization of wet gas compression at Gullfaks C will lead to an increased recovery of 22 million barrels of oil equivalent (BOE) as well as an extended plateau production of two years [1]. At the current oil price of 40USD/BOE this amounts to an additional income of 880 million USD. Figure 1.1 depicts one of the few operating subsea wet gas compressors, stationed at Gullfaks C.

Despite subsea wet gas compression showing several desirable attributes, it is still a relatively new technology thus possessing a degree of uncertainty of operation. Introduction of liquid in the compression process greatly increases the operation complexity. Wet gas compressors are, in the same way as dry gas compressors, prone to degradation mechanisms such as fouling. As of now, the effect of fouling in wet gas compression is not well understood. It is essential that this deteriorating mechanism is further investigated in order to reduce the uncertainties connected with wet gas compression.

Economical as well as environmental aspects require the compressor to operate at peak performance. Understanding the shift in compressor performance for different degrees of fouling and its effect in combination with varying GMFs will be essential for optimization of the compressor operation as well as condition monitoring. The highly developed NTNU wet gas compression test facility allows for investigation of both dry and wet gas behaviour and its response to fouling.



Figure 1.1: Gullfaks C wet gas compressor [2].

1.2 Scope of Thesis

Compressor operating experiences document a certain performance deterioration after some thousand running hours. Material build-up on the compressor internals, also known as compressor fouling, is one of the primary deteriorating mechanisms in compressor operations. An improved understanding of how narrowing of the flow path and increased roughness affects the compressor at dry and especially wet gas conditions is needed. Based on literature review and experimental work at the NTNU compressor lab facility, the focus areas are the following:

- 1. Establish relevant compressor performance characteristics.**

By this it is meant to obtain clean performance curves for the NTNU wet gas compressor for dry and wet conditions to serve as references for the fouling tests.

- 2. Review and establish relevant diffuser fouling scenarios.**

Information gathering regarding fouling, and particularly with respect to the diffuser section, is needed to give insight to different parameters to be replicated. “Establish relevant diffuser fouling scenarios” refers to both establishing the method of replication as well as different scenarios to be tested eg. different roughness and/or thickness.

3. Test and document how different diffuser fouling affects the dry and wet performance characteristics.

The effect of the adopted diffuser fouling method from point 2 on the compressor characteristics will be tested for the same GMFs as in point 1 to be compared.

1.3 Limitations of Scope

Scope 1 & 3: The effect of fouling on the compressor characteristics for dry and wet conditions has been limited to stable operating conditions. Only steady state values will be utilized in the calculations for the fouled and clean test conditions. Transients like surge and rotating stall has not been part of the scope of this master's thesis.

Scope 2: The experimental test period was significantly reduced as a result of the COVID-19 lockdown of NTNU and the wet gas compression test facility. This made for testing of different degrees of fouling thickness and roughness not feasible within the time frame of the new test period. In accordance with recommendations from Lars Eirik Bakken (supervisor) regarding the new test campaign, only a single fouling scenario with its respective roughness and thickness was tested for the fouled compressor tests.

In order to preserve the transparency of the Plexiglas diffuser shroud during testing, reduce the risk of scratching during the removal process and chemical reactions compromising its integrity, the application of the fouling replica was restricted to the diffuser hub only.

1.4 Information Retrieval

This thesis aims to contribute to an enhanced understanding of compressor deterioration resulting from fouling. An extensive literature review has been conducted, both in the author's pre-master's project and the current master's thesis. The literature review served to give an understanding of existing knowledge in addition to assist in predictions and planning associated with the experimental campaign.

Focus has been directed towards obtaining relevant and reliable information during the literature review. Information has been acquired from databases with peer-reviewed journals, relevant books, handouts, subject-specific professional websites, in addition to previous thesis' written at NTNU. A large portion of the information is gathered from the databases: "Google scholar" and "The American Society of Mechanical Engineers" (ASME). Effort has been put into applying structured search patterns for both databases, where different keyword and respective synonyms have been checked.

Being a relatively new technology, literature and experience within wet gas compression are limited. A significant share of the research regarding wet gas compression has thus

been obtained from the state-of-the-art NTNU wet gas compression facility. How fouling in combination with changes to the GMFs has, to the author's knowledge, only been studied by Paulsen and Haugen [3] for the inducer section. Information on dry gas fouling has been investigated for the diffuser section, but also other components. This has been done due to few documentation regarding the effect of diffuser fouling.

Some of the theory in the chapters regarding compressor fundamentals and compressor fouling, in addition to the compressor rig setup, are based on the author's own pre-master's project [4]. The chapters are updated and improved to fit the current scope of the thesis.

1.5 Report Structure

The master's thesis is structured in the following way:

1. Chapter 1 – Introduction of the thesis' objective and background, its scope with its subsequent limitations, in addition to a brief summary of the information retrieval process.
2. Chapter 2- Presentation of centrifugal compressor fundamentals, compressor and fouling losses, liquid impact and, dry and wet gas polytropic performance.
3. Chapter 3 – Introduces fouling fundamentals with respect to entrainment and sticking mechanisms, in addition to documented effects of fouling on different compressor components for both dry and wet conditions. A brief introduction to the Reynold correction method and an adaptation aimed to correct for fouled conditions are also presented.
4. Chapter 4 – Presents the attributes of fouling obtained from industry and in-house samples to be replicated. Reviewed fouling replication techniques, the adopted technique and diffuser fouling scenario are also presented. The procedure for obtaining the fouling replica in addition to the application and removal process are also covered.
5. Chapter 5 - Presents the experimental test campaign, the NTNU wet gas test facility, test procedure, data processing and uncertainties.
6. Chapter 6 – Presents the obtained results from the conducted experimental campaign and calculations, and discussion of these.
7. Chapter 7 - Conclusion based on the experimental campaign and recommendations for further work.

Compressor Fundamentals

The following chapter introduces the reader to compressor fundamentals. Operational principles, compressor characteristics and performance, as well as compressor losses affected by fouling will be described. The implications and changes to the compressor's operational performance when moving from dry to wet gas scenarios will be highlighted.

The NTNU compressor facility operates with a single stage compressor with backswept impeller blades and vaneless diffuser. The theoretical focus and literature review have thus been, to the extent possible, directed towards similar centrifugal compressor setups.

2.1 Operational Principles

A compressor is a machine used to increase the pressure of a gaseous fluid by energy transfer and energy conversion. An illustration of a single stage centrifugal compressor with its main parts and corresponding velocity triangles can be seen in Figure 2.1. The working fluid enters the impeller through the compressor inlet. Through the impeller energy is transferred to the fluid by whirling it outwards, thus increasing its angular momentum. Both the static pressure and the fluid velocity are increased through the impeller section [5]. Through the radial diffuser the tangential velocity is reduced due to conservation of angular momentum. This results in kinetic energy of the flow being converted into pressure energy. After passing through the diffuser section, the flow is collected in the volute and delivered to outlet pipes. The curved impeller surface, a-b, is known as the hub and the curved surface c-d is known as the shroud. Similarly, corresponding sides of the diffuser are either referred to as the hub or shroud side.

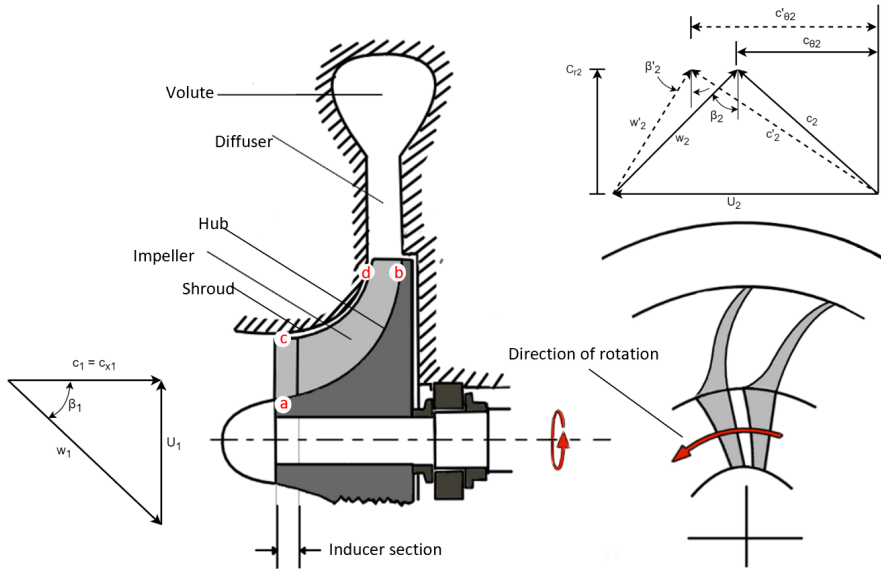


Figure 2.1: Overview of backswept centrifugal compressor with corresponding velocity triangles.

2.1.1 Theoretical, Ideal and Actual Head

The theoretical head, also known as the Euler head, delivered by the compressor is a function of the compressor geometry and rotational speed. If the velocity triangles are known, the Euler head can be computed from Equation 2.1. At design point there is no inlet swirl, thus yielding $c_{\theta 1}$ equal zero.

$$H_t = U_2 c_{\theta 2} - U_1 c_{\theta 1} \quad (2.1)$$

The flow will experience slip at the trailing edge of the impeller blades resulting from the pressure difference on the two sides of the blade. This causes the relative outlet flow angle, β_2 , being greater than the outlet blade angle, β'_2 , and a reduction in $c_{\theta 2}$ follows. The effect of slip changing the relative outlet angle would still be present in inviscid flow and gives the ideal head. In real compressor operations several loss mechanisms further reduce the performance and give rise to the actual compressor head. A representation of the different compressor heads are visualized in Figure 2.2.

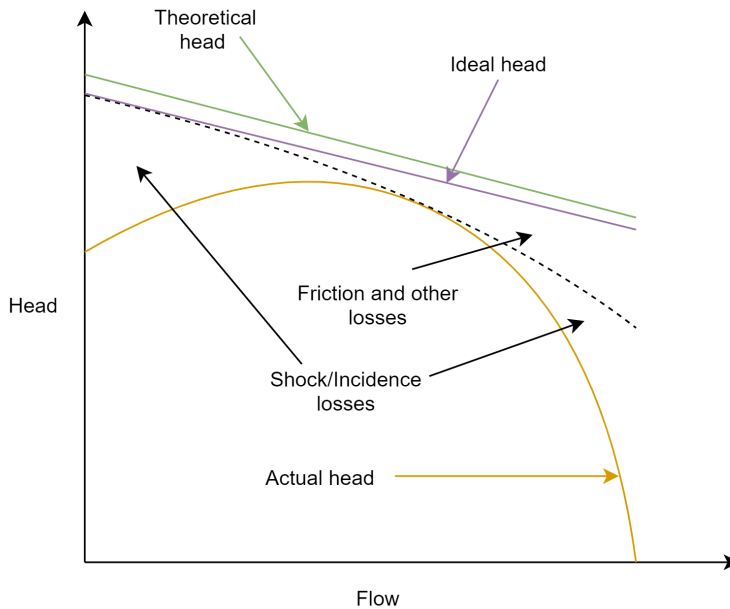


Figure 2.2: Graphical representation of the theoretical, ideal and actual head with corresponding losses for backswept centrifugal compressor.

2.1.2 Compressor Maps and Characteristics

The operational regime of a compressor is often graphically displayed in the form of a compressor map. The compressor map consists of a collection of different compressor curves, corresponding to different rotational speeds for the given compressor. For centrifugal compressor operations, the compressor map is often presented with either; discharge pressure, polytropic head or pressure ratio plotted against suction volumetric flow rate. These curves display the compressor performance and are thus often referred to as the compressor characteristics. A visualization of a compressor map can be seen in Figure 2.3.

The intersection between a compressor curve and the optimum efficiency line is referred to as the curves best efficiency point (BEP). The location of the BEP with regards to inlet suction flow rate can be seen shifting towards lower flow rates for descending rotational speeds. Constant efficiency lines can be seen surrounding the optimal efficiency line and indicating the efficiency of the different points of the curves.

The characteristic curves in the compressor map in Figure 2.3 can be seen defined to the right by the choke line which restricts the maximum compressor throughput. During choked conditions, the flow Mach number reaches unity at some location in the compressor. This means that no further increase in mass flow is possible by reducing the back

pressure assuming constant inlet parameters. This can be seen by the vertical slope on the compressor curve for high flow rates.

The operational domain of the compressor map is seen defined to the left by the surge line. The surge point equates to the maximum pressure the compressor is able to provide and a reduction in flow rate from this point will cause compressor instability. When the flow is reduced below the surge limit, to point A the discharge pressure exceeds that of what the compressor is able to provide. The occurring pressure difference results in a temporary reversal of the flow. This is seen as the jump from A to B as the operating point is unable to reside on the curve segment A-C. Due to the reversal of the flow, the discharge pressure decreases, and the operating point moves from B to C. Unable to exist on the curve segment A-C the operating point jumps to point D. If no changes is made to the flow throttle valve the operating point will travel towards point A and the cycle continues [6]. The transient and dynamic loads associated with surge can result in substantial damage to the compressor.

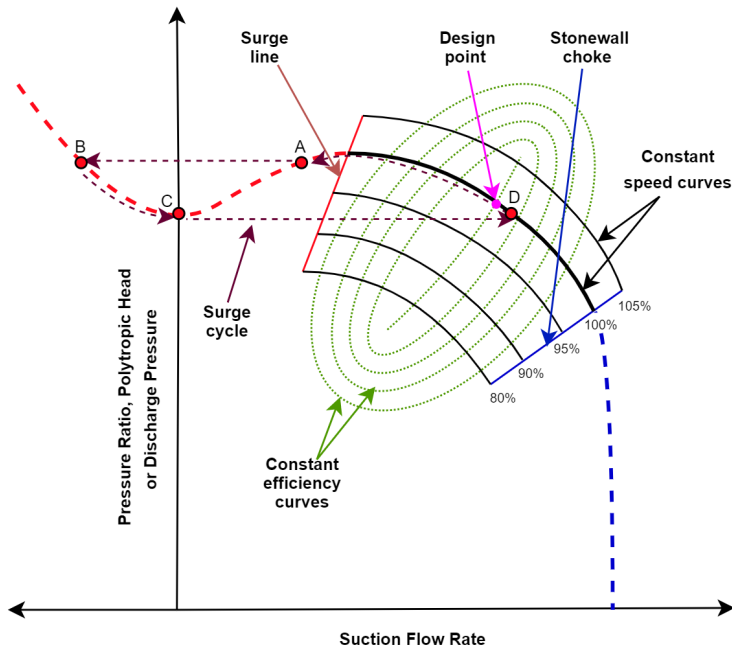


Figure 2.3: Centrifugal compressor map where the the operational domain, surge and choked operations are visualized for a compressor curve.

2.1.3 Head Rise to Surge

Having a continuous and positive head rise towards the surge point when reducing the volume flow is important to ensure sable and reliable operation. Head rise to surge (HRTS)

is a measurement of the ratio between the surge head and the head of an operating point. The compressor head slope governing the HRTS is a function of the aerodynamic design and geometry of the compressor. The HRTS can be given as a percentage as shown in Equation 2.2. Other commonly used terms related to HRTS includes: “pressure rise to surge” and “pressure ratio rise to surge” [7].

$$HRTS = \left(\frac{H_{p,s}}{H_{p,OP}} \right) \times 100 \quad (2.2)$$

2.2 Compressor Losses

The losses connected to compressor operation and their magnitude depend on several factors including, the compressor type, operating fluid and operational parameters. Several different loss mechanisms exist for compressor operation, but in this section only the losses effected by fouling will be presented. Mechanical losses and leakage losses are thus assumed unchanged for fouled conditions and will not be discussed.

Fouling of compressor internals will result in an increase in surface roughness, affect flow turning properties, as well as reduce the effective flow area. Compressor fouling introduces challenges when trying to quantify the additional losses due to changes in pressure ratio, mass flow and efficiency [8]. Wet gas compression introduces additional losses and complexity that at present time is not fully understood. Thus, the loss models presented will be for single phase gas compression in order to illustrate how changes in parameters due to fouling affects the losses.

2.2.1 Skin Friction Losses

Losses generated by shear forces resulting from a relative velocity between a viscous fluid and a surface is known as skin friction losses. The magnitude of the losses is dependent on the viscosity of the fluid, the thickness of the viscous boundary layer, the surface roughness and velocity profile. As the boundary layer thickness is related to the Reynolds number, so is the friction factor. For single phase flow, the friction factor can be obtained from the moody diagram when the relative surface roughness and the Reynolds number are known. Aungier [9] introduced Equation 2.3 to approximate the skin friction losses of the impeller where \bar{w} is computed from Equation 2.4.

$$\Delta q_{sf} = 2\lambda \left(\frac{\bar{w}}{U_2} \right)^2 \frac{L}{d_h} \quad (2.3)$$

$$\bar{w}^2 = \frac{w_1^2 + w_2^2}{2} \quad (2.4)$$

The flow of the centrifugal compressors covered in this master's will primarily operate in fully turbulent flow. The friction factor, λ , can be extracted from the Moody diagram or obtained from Equation 2.5.

$$\frac{1}{\sqrt{4\lambda}} = -2\log_{10} \left(\frac{e}{3.71d_h} \right) \quad (2.5)$$

From Equation 2.5 it is evident that the friction factor, λ , increases during compressor fouling as the peak-to-valley surface roughness, e , is increased. The change in skin Δq_{sf} is seen proportional to the change in λ .

2.2.2 Blockage Losses

Compressor fouling causes material build up inside the compressor thus reducing the effective flow area. The deposited material will also increase 3D separation and increase displacement thickness of the flow due to earlier turbulent transition. The losses connected with the reduction in effective flow area are known as blockage losses [8].

2.2.3 Incidence Losses

The losses connected to the flow entering the inducer and impeller section with an angle relative to the blade angle are called incidence or shock losses. The relative angle causes the flow to collide with the blades. Adherence of particulate matter on the leading edge of the blades can alter the optimal flow angle thus resulting in increased incidence losses. A reduction in the flow rate resulting from fouling can also effect the incidence losses as the relative inlet angle gets altered. Equation 2.6 given in [9] can be used to obtain the incidence loss in the impeller.

$$\Delta q_{inc} = 0.4 \frac{\left(w_1 - \frac{c_{x1}}{\sin \beta_1} \right)^2}{U_2^2} \quad (2.6)$$

From the equation it is evident that the described effect of fouling altering the inlet blade angle or reducing the flow rate will affect the incidence losses.

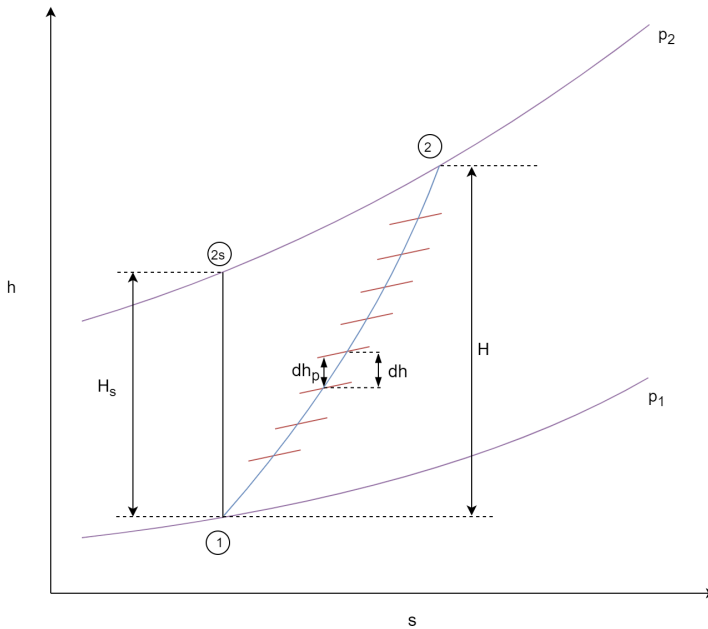


Figure 2.4: Graphical representation of the polytropic compression path.

2.3 Dry Gas Polytropic Performance

In order to reliably predict real gas compressor performance – a precise thermodynamic evaluation is required. Utilization of a polytropic analysis is often preferred to the isentropic analysis, especially for variations in operating conditions and high pressure analysis [10]. In both ASME PTC-10 [11] and ISO 5389 [12], the polytropic analysis is based on the method developed by Schultz [13]. A description of Schultz method can be found in Appendix A - Schultz Method.

A polytropic compression process relates to infinitely small isentropic compression steps along the actual compression path. The path is governed by the polytropic efficiency of the process. Due to the diverging nature of the isobars at elevated temperatures, as seen in Figure 2.4, the polytropic head will always be greater than the isentropic head. The polytropic process at constant efficiency is often defined by the path expression given by Equation 2.7.

$$pv^{n_v} = const \quad (2.7)$$

Along the compression path the polytropic temperature exponent, n_T , and volume exponent, n_v , may change. The approximation of the polytropic head in Equation 2.8 assumes

constant polytropic exponents. Schultz [13] presented a correction factor, f , to account for the errors resulting from this approximation (See Appendix A - Schultz Method). Schultz's correction of the polytropic head can be seen in Equation 2.9. When both the polytropic head and total head are known, the polytropic efficiency can be calculated from Equation 2.10.

$$H_p = \int_1^2 v dp \approx \frac{n_v}{n_v - 1} \frac{Z_1 R_0 T_1}{MW} \left[\left(\frac{p_2}{p_1} \right)^{\frac{n_v - 1}{n_v}} - 1 \right] \quad (2.8)$$

$$H_p = \int_1^2 v dp \approx f \frac{n_v}{n_v - 1} \frac{Z_1 R_0 T_1}{MW} \left[\left(\frac{p_2}{p_1} \right)^{\frac{n_v - 1}{n_v}} - 1 \right] \quad (2.9)$$

$$\eta_p = \frac{H_p}{H} \quad (2.10)$$

2.4 Liquid Impact

Introducing liquid to the compressor flow heavily affects the compressor performance and normal dry gas polytropic relations will not be valid [14]. This section gives an introduction to wet gas compression by familiarizing the reader with basic wet gas parameters, multiphase effects and wet gas polytropic performance.

2.4.1 Energy Transfer

The presence of liquid causes the multiphase density to be greater than that of dry gas, thus reducing the volume flow rate for a given mass flow rate. A decrease of the volumetric flow rate corresponds to a reduction in c_{r2} . As the time spent in the impeller increases, more energy is transferred to the flow thus increasing $c_{\theta 2}$. The changes to the impeller outlet velocity diagram can be seen in Figure 2.5. From Equation 2.1 we can see that the theoretical head increases. Despite the increase in the theoretical head, the actual head is reduced due to increased losses. The main losses mechanisms connected with multiphase flow will be presented in Subsection 2.4.3.

2.4.2 Basic Wet Gas Parameters

In wet gas compression the ratio between gas and liquid at the compressor inlet is either given by the gas volume fraction (GVF) or the gas mass fraction (GMF). The GVF relates to the flow field characteristics while the GMF relates to the pressure increase and power

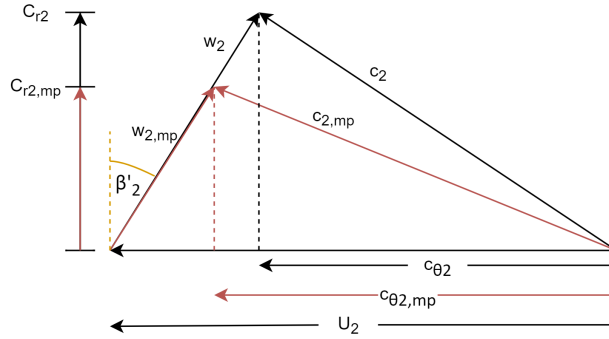


Figure 2.5: Change in impeller outlet velocity triangle resulting from liquid introduction.

consumption. Wet gas compression is considered suitable for a GVF range from 95%-100% [15]. The GVF and GMF can be computed from Equations 2.11 and 2.12.

$$GVF = \alpha = \frac{Q_g}{Q_g + Q_l} \quad (2.11)$$

$$GMF = \gamma = \frac{\dot{m}_g}{\dot{m}_g + \dot{m}_l} \quad (2.12)$$

The *density ratio*, δ , indicates the degree of homogeneity in the fluid mixture as well as the slip between the phases. The droplets ability to respond to changes in the gas flow is also dependent on this ratio.

$$\delta = \frac{\rho_g}{\rho_l} \quad (2.13)$$

The complexity of multiphase compression can be reduced if the flow can be regarded as homogeneous. The mixture can then be regarded as a single fluid with a multiphase density, ρ_{mp} which can be calculated using Equation 2.14

$$\rho_{mp} = \alpha\rho_g + (1 - \alpha)\rho_l \quad (2.14)$$

2.4.3 Multiphase Effects on Compressor

The presence of liquid in the compressor stream introduces multiphase effects not present in normal dry gas compression. The liquid alters aerodynamic shapes, increases losses and affect the thermodynamic behavior of the compressed fluid due to phase interactions. Some of the multiphase effects occurring in wet gas compression is presented below [14]:

Evaporative cooling / condensing heating: Wet gas compression may experience a reduction in the gas discharge temperature compared to dry gas scenarios. The droplets lower the gas temperature by absorbing energy through evaporation. The effect is similar to intercooling between compressor stages, thus lowering the theoretical specific power consumption. In rare cases the opposite effect of condensing heating can be experienced through the compressor. The non-equilibrium between the phases results in heat, mass and momentum transfer between the phases resulting in increased losses.

Heat transfer: Cooling of the gas phase can still occur without evaporation due to the temperature difference between the gas and liquid phase. The liquid experiences a smaller temperature increase through the compressor compared to the gas resulting from its higher heat capacity. Due to the temperature difference, heat transfer between the phases lowers the gas temperature.

Density change: Owing to the high density of the liquid, even small quantities of liquid would greatly affect the mixture density as seen from Equation 2.14.

Liquid film: The formation of liquid films on compressor components increases the roughness interacting with the gas phase due to formation of small waves on the film surface. The film results in increased frictional losses in the gas in addition to increased frictional losses between the compressor surface and the liquid film. How this effect couples with fouling is not well documented. Similarly to fouling related blockage, the effective flow area is reduced due to increased displacement thickness in addition to the physical presence of the liquid film [16].

Liquid entrainment/deposition: : High velocities in compressor stream promotes droplet entrainment through liquid atomization. The acceleration of the entrained droplets reduces the kinetic energy in the high velocity gas-liquid flow core. The kinetic energy of the high velocity gas-liquid flow core is further reduced when droplets at high velocity get deposited in the slower moving liquid film.

Inertial impaction: Water droplets will impact in areas possessing high degree of flow turning due to the droplets high Stokes number. Particles possessing larger Stokes numbers are less reactive to pressure changes in the flow and tend to follow their initial trajectory. This results in the liquid particles impacting on the pressure side of the blades causing losses as a result of abrupt change in direction. The stokes number for a particle is given by Equation 2.15.

$$Stk = \frac{(\rho_{par} d_{par}^2)/(18\mu_g)}{\tau} = \frac{\text{Particle response time}}{\text{Fluid response time}} \quad (2.15)$$

2.5 Wet Gas Polytropic Performance

Currently there exists no standard for the evaluation of wet gas compressor performance. However, the compression path, similar to that of dry gas, is given by the polytropic efficiency. The **two fluid model** is a simplified calculation method for two phase flow where there is assumed no interactions or transport between the phases. As described in Subsection 2.4.3 this is not valid, but the method provides an estimation. The two fluid polytropic head is given by:

$$H_{p,mp} = \gamma \frac{f n_v}{n_v - 1} \frac{Z_1 R_0 T_1}{MW_g} \left[\left(\frac{p_2}{p_1} \right)^{\frac{n_v - 1}{n_v}} - 1 \right] + (1 - \gamma) \left[\frac{p_2 - p_1}{\rho_l} \right] \quad (2.16)$$

A more realistic model is the **total fluid model** which includes the properties of both gas and liquid. The model is similar to that of Schultz method for dry gas but operates with multiphase properties. Special care should be taken when the fluid contains water and/or MEG as many of the normally utilized equations of state may give unreliable property data [10]. The total fluid polytropic head is given by:

$$H_{p,mp} = f_{mp} \frac{n_{v,mp}}{n_{v,mp} - 1} (p_2 v_{2,mp} - p_1 v_{1,mp}) \quad (2.17)$$

The multiphase correction factor, f_{mp} , is similar to the correction factor given in Appendix A - Schultz Method but utilizes the multiphase properties. The correction factor is given by:

$$f_{mp} = f_{s,mp} = \frac{h_{2s,mp} - h_{1,mp}}{\frac{\kappa_{v,mp}}{\kappa_{v,mp} - 1} (p_2 v_{2s,mp} - p_1 v_{1,mp})} \quad (2.18)$$

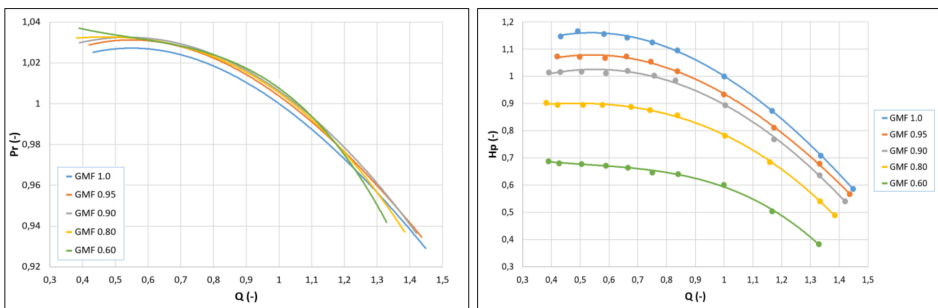
The polytropic volume exponent, $n_{v,mp}$ is given by:

$$n_{v,mp} = \frac{\ln \left(\frac{p_2}{p_1} \right)}{\ln \left(\frac{v_{1,mp}}{v_{2,mp}} \right)} \quad (2.19)$$

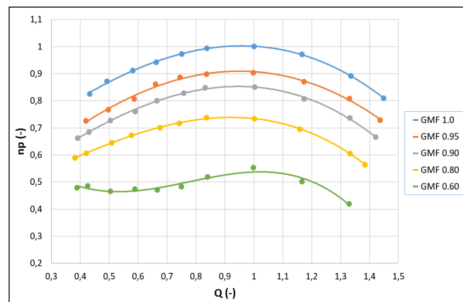
When the polytropic multiphase head as well as the total multiphase head is known, the polytropic multiphase efficiency can be computed by the following equation:

$$\eta_{p,mp} = \frac{H_{p,mp}}{H_{mp}} = \frac{\dot{m}_{mp} H_{p,mp}}{P_{fluid,mp}} \quad (2.20)$$

Hundseid et al. [14] studied the performance of high pressure wet gas compression with hydrocarbon condensate representative of that in the North Sea. The study displays a reduction in both polytropic head and efficiency but an increase in pressure ratio with descending GVF. Similar trends have been found by Bakken et al. [17], and Paulsen and Haugen [3] at the NTNU compressor test facility operating with water and air at low inlet pressure. Figures 2.6a-c display the compressor characteristics where the normalized pressure ratio, polytropic head and efficiency are plotted against a normalized suction volumetric flow rate for different GMFs. The normalization has been performed towards the BEP at GMF = 1. It can be seen from Figure 2.6a that liquid introduction increases the pressure ratio but the increase does not vary significantly with the GMF. The polytropic head and efficiency curves in Figure 2.6b and 2.6c are in contrast to the pressure ratio curves substantially reduced for increased liquid content.



(a) Normalized pressure ratio curves for different GMFs. (b) Normalized polytropic head curves for different GMFs.



(c) Normalized polytropic efficiency curves for different GMFs.

Figure 2.6: Compressor characteristic curves for different GMFs ranging from 1 to 0.6 with water and air as the operating fluids [17].

2.6 Summary

In this chapter compressor fundamentals as well as increased losses resulting from compressor fouling has been presented. Two important elements covered in this chapter are the change in compressor performance and the multiphase effects resulting from liquid in the compressor stream. Liquid introduction in the gas stream introduces several effects not present in dry gas compression. These include evaporative cooling, heat and momentum transfer, liquid film formation, density change, liquid entrainment/deposition and inertial impaction. Several sources document a reduction in the polytropic head and efficiency but an increase in pressure ratio for wet gas compression.

Compressor Fouling

Compressor fouling is a degradation phenomenon caused by particles or impurities present in the gas stream adhering to both rotating and stationary part of the compressor. The material build-up from compressor fouling may alter the aerodynamic shape of airfoils, change the inlet and outlet angles, increase surface roughness on compressor components and reduce the effective flow area [18]. Consequently, the compressor performance is reduced due to an increase of the losses. The following chapter gives an introduction to the governing fouling mechanisms in compressor operation with regards to entrainment and sticking mechanisms, as well as the effect of fouling on compressor operations. In addition, an adaptation of the Reynold correction method aimed to account for fouling is presented.

3.1 Fouling Mechanisms

All compressors are susceptible to fouling. The degree and rate of fouling, and the effect on the performance depends on several parameters including: compressor design, operational environment, surface smoothness/coating, compressing fluids and particulate matter in the process stream. Kurz and Brun [19] proposed that fouling mechanisms should be distinguished between the following:

- Entrainment mechanisms: How particles of various sizes reach the compressor surface.
- Sticking mechanisms: How the particles that reach the surface end up sticking to the surface.

- The loss mechanisms associated with the material buildup and how it affects the compressor performance.

3.2 Entrainment

The three governing entrainment mechanisms for particles in compressor flow are diffusion, interception and inertial impaction. Smaller particles in the range of $1\ \mu\text{m}$ and smaller are dominated by diffusion. Larger particles in the range of $5\text{-}10\ \mu\text{m}$ are more influenced by interception and inertial impaction [19]. The different entrainment mechanisms can be seen in Figure 3.1.

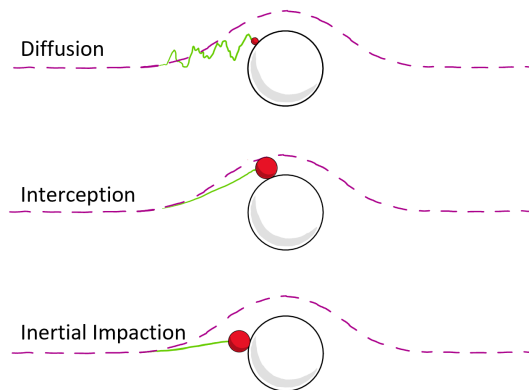


Figure 3.1: Representation of the governing compressor fouling entrainment mechanisms.

Diffusion

Smaller particles will have a strong tendency to follow the streamlines of the flow as a result of their low Stokes number. Mass transport perpendicular to the streamlines is thus highly dependent on diffusion. For compressor operations, laminar diffusion can be neglected and turbulent diffusion is the primary diffusion mechanisms. Turbulence greatly amplifies the mass transfer perpendicular to the streamlines through eddy diffusion. This causes a higher concentration gradient near the viscous sub layer than for laminar diffusion and thus a higher mass transfer to the surface [20].

Inertial Impaction

The mass transfer to the compressor surface for flows containing larger particles, and especially wet gas compression, will be heavily contributed by inertial impaction. Owing to their size, the larger particles will have a higher Stokes number. This causes them to be less susceptible to changes in the flow and rather follow their initial trajectory. As a result, the particles collide with the surfaces [19] [21]. This mechanism will therefore be most influential in areas of the compressor possessing flow turning properties. Centrifugal compressor components having high degrees of flow turning include inducer and impeller blades, inlet guide vanes (if any), diffuser vanes (if any) and return bends.

Several experiments have been conducted focusing on particle deposition on axial turbine and compressor blades ([22], [23], [24], [25]) and more). Syverud et al. [23] studied the formation of deposits on two multistage axial compressors subjected to saltwater in the flow. She found that the most severe deposits were localized at the first stage anulus, the leading edge of the second stator and the pressure side of the second- and third-stage blades and vanes.

Sun et al. [26] studied the deposition of oil droplets on the diffuser section of a centrifugal vehicle turbocharger compressor. The numerical simulation analysed the quantity and location of the particles impacting the diffuser walls. The hub side of the diffuser displayed a substantially larger mass transport to the surface resulting from inertial impaction of the oil particles at inner radiuses. The mass transfer to the surface was seen decreasing with increasing radiuses as inertial impaction became less pronounced and diffusion became the dominant entrainment mechanism. The mass transfer to the shroud side was primarily governed by diffusion. The results from Syverud et al. and Sun et al. correlate well with the described effect of inertial impaction being dominant in flow turning regions.

Interception

Kurz and Brun [19] states that mass transfer through interception can be neglected for axial compressor blade. They base the statement on mass transfer mechanisms in heat exchanger pipe flow to be representative for the flow over axial compressor blades. They refer to a study on the deposition of particles in a heat exchanger tube flow, performed by J. A. Siegel in his Ph.D. thesis "Particulate Fouling of HVAC Heat Exchangers" from 2002, where the interception mechanism was not prominent compared to diffusion and inertial impaction.

Both heat exchanger pipe flow and the blades on axial compressors possess a high degree of flow turning properties resulting in larger particles being more prone to inertial impaction. It is not clear if the interception mechanism can be neglected for the diffuser section as the diffuser walls are parallel and display little flow turning properties. Apart from this study there is little emphasis on the interception mechanism in literature and will therefore not be discussed further.

3.3 Sticking Mechanisms

Whether or not a particle impacting on the compressor surface becomes stationary depends on the balance between the adherence and dislodging forces acting on the particle [27]. Smaller dry particles are more likely to stick to a surface than larger ones. Introduction of liquid increases the likelihood for both smaller and larger particles to stick to the impact area [28]. For hydrocarbon processing equipment, polymerization is the main contributor to fouling. Materials in the process stream change from gas or liquid phase to either adhesive or abrasive polymers. The adhesive polymers will then stick to internal surfaces in the compressor or already formed deposits. The chemical mechanisms present in polymerization of hydrocarbons during compressor operations are complicated and not well understood [29]. In the book, “A practical guide to compressor technology”, by Heinz P. Bloch [6], several key factors that have been empirically established to enhance fouling rates in compressors are presented. They are the following:

- Temperature: Polymerization occurs above 90°C (194° F).
- Pressure: The degree of fouling is proportional to the pressure.
- Surface finish: The smoother the surface, the less receptive the component is to fouling
- Gas composition: Fouling is proportional to the concentration of reactable hydrocarbons in the process gas

Haq and Bu-Hazza [30] investigated improvements of a fouled centrifugal compressor train operating in an ethane cracked gas environment. They highlight the effect of temperature and pressure on the fouling rate, but also the impact of heavier more reactive hydrocarbons. By heavier hydrocarbons Haq and Bu-Hazza refers to C5 plus, butanes, butenes, butadiene, propane, propylene and propadiene. Deposits of the heavier ends were particularly observed in the fouling material collected from the machine despite low concentrations in the process stream.

Despite a substantial mass transfer by inertial impaction to the leading edge and pressure side of the impeller blades, relatively little fouling is observed. In the results from Syverud et al. [23] the impeller was not observed to foul significantly despite possessing flow turning properties. It was suggested that the low degree of fouling was a consequence of centrifugal forces acting on the particles on the blades. This complies with [6] that states that rotating compressor elements are less prone to fouling due to the dynamic and dislodging forces acting on the deposits. It also mentions that rotating compressor components often have a smoother surface finish than stationary components which further improves fouling resistance. A retired centrifugal compressor at the NTNU test facility, previously operating at Åsgard, display the same trends. The compressor exhibits a significant difference in the deposit quantity for the impeller and diffuser section. A visual of the compressor can

be seen in Figure 3.2. It is evident that that the diffuser is more affected by fouling than the impeller section.



Figure 3.2: Close up of impeller and diffuser hub side of a multistage hydrocarbon compressor previously operating at Åsgård.

There is, unfortunately little information available on the effect wet gas has on the fouling rate. Brenne et al. [31] conducted an experiment to document the performance of a wet gas compressor. The compressor was operated with a hydrocarbon mixture with GVFs ranging from 1 to 0.97. From the tests it was observed that the condensate had cleaned the internals of the compressor after the 300 operating hours. In contrast to this, Brenne et al. [32] discovered that single phase compressors operating with an upstream scrubber were susceptible to fouling resulting from liquid carryover from the scrubber. The droplets would collect contaminants in the flow and evaporate through the machine, thus depositing the material.

3.4 Effect of Compressor Fouling

When operating a compressor in a challenging environment such as wet hydrocarbon gas compression, it is essential to understand the shift in operational performance due to different deteriorating mechanisms. Understanding how the different compressor components react to fouled conditions are therefore of great importance. However, there is little information on the effect of fouling in combination with wet gas compression, so most of the obtained information in this section are from dry gas compression.

3.4.1 Inducer

Paulsen and Haugen [3] tested the effect of fouling the inducer blades of a centrifugal compressor operating in a GMF range of 1 to 0.9. Emery cloth reinforced by an epoxy

layer at the leading edge to enhance wet gas durability was glued to the inducer blades to imitate fouling. The thickness of the fouling replica was kept constant while the roughness was altered by changing between emery cloth grit sizes.

The fouled tests were compared to their respective unfouled baselines for the different GMFs and displayed a clear reduction in performance parameters such as pressure ratio, polytropic head and polytropic efficiency. The largest degradation was observed for the roughest fouling replica at maximum flow rate. There was also observed a reduction of the throughput of the compressor resulting in a reduction in the operational domain. The BEP was observed reduced and shifted towards lower flow rates. The relative reduction in polytropic head and efficiency were increased with increasing flow rates.

Presented bellow are the obtained results by Paulsen and Haugen for the least rough coating (P150) as the baseline test for GMF 0.975 was not tested for the roughest coating. The results will serve as important comparing references as it is, to the author's knowledge, the only source to document wet gas fouling.

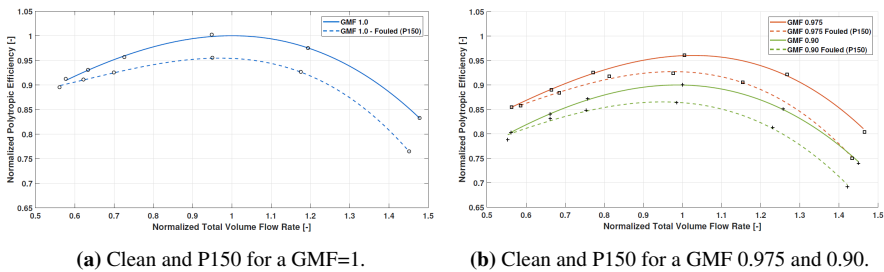


Figure 3.3: Dry and wet gas normalized polytropic efficiency plotted against normalized total volume flow rate for both clean and fouled conditions [3].

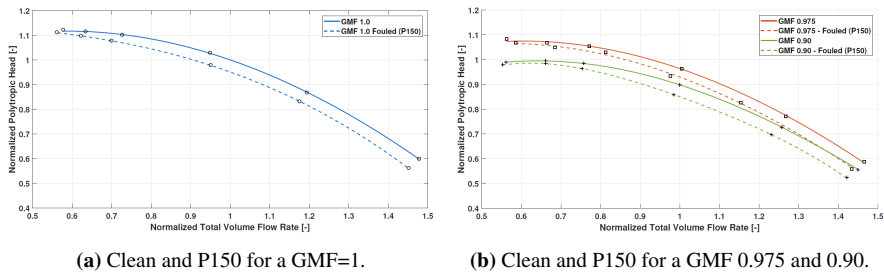


Figure 3.4: Dry and wet gas normalized polytropic head plotted against normalized total volume flow rate for both clean and fouled conditions [3].

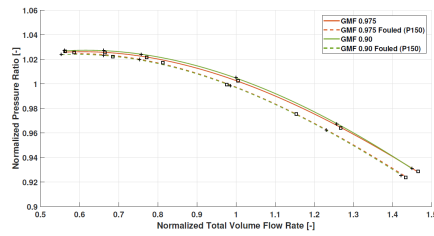
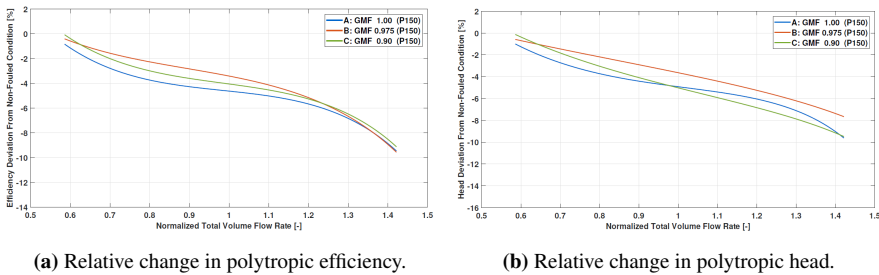


Figure 3.5: Normalized pressure ratio for GMF 0.975 and 0.90 plotted against normalized total volume flow rate for both clean and fouled conditions [3].



(a) Relative change in polytropic efficiency.

(b) Relative change in polytropic head.

Figure 3.6: The relative change in polytropic efficiency and head when going from clean to fouled condition for GMF 1, 0.975 and 0.90 [3].

3.4.2 Impeller

Al-Busaidi and Pilidis [33] stated that fouling effects a centrifugal compressor through three main mechanisms: an effective area reduction, increase in the frictional losses, and flow and pressure profile distortion. The narrowing of the flow path increases the velocity and coupled with higher surface roughness results in increased blockage and frictional losses. The increased velocity through the impeller section results in a reduction in the energy transfer to the flow. This can be seen by a reduction in the tangential velocity component, $c_{2\theta}$, resulting from the increase in the radial velocity component, c_{2r} . A reduction in the flow area can also create a non-stable flow region yielding higher amounts of internal recirculation and a random distribution of the pressure on the blade. An alteration in the flow pattern and velocity distributions will come as a result of this, resulting in increased losses in the flow.

Ju and Zhang [34] performed CFD simulations on a centrifugal impeller for both fouled and unfouled dry gas conditions in order to study the shift in aerodynamic performance. Fouling was simulated by applying a randomized fouling map to the impeller surfaces to simulate the uneven and random nature of the material build-up. It was found that fouling of the impeller section resulted in a degradation of the compressor performance with a reduction in both polytropic efficiency as well as the pressure ratio. The reduction was

found, similarly to that described by Haugen and Paulsen [3], to be more severe for higher flow rates. A sensitivity analysis was also carried out with regards to increased roughness. It showed that a roughness increase at the leading edge of the impeller blades had the greatest impact on the impeller performance degradation.

3.4.3 Diffuser

To the author's knowledge there are few experimental reports connected to compressor diffuser fouling. Extensive research in the field of diffusers has been conducted but mainly related to diffuser stall and dimensioning towards the impeller section. Although rotating stall in the diffuser is dependent on the velocity field leaving the impeller, which can be influenced by fouling in the diffuser or other parts, the phenomena of diffuser stall is of an unsteady nature and not part of the scope for this master's thesis.

Haq and Bu-Hazza [30] investigated the effect of fouling on both impellers and diffusers when modeling and analyzing a severely fouled compressor train operating with cracked ethylene. The analysis showed a significantly larger reduction in the diffuser efficiencies due to fouling than that of the impeller efficiencies over the 27 stages. It should be noted that the impeller and diffuser sections did not possess the same degree of material build up, but the results portray the efficiency reduction of a compressor train that operated for 11 years without any major overhauls to the system. In order to meet the required mass flow rate, the inlet pressure of the modelled compressor train was raised during the operation period. This indicates a reduction in the volumetric flow rate due to fouling and thus a narrowing of the operational domain of the compressor train. It was concluded that fouling of early compressor stages, and especially the diffuser section, had a big impact on the efficiency of the later stages of the compressor.

Despite a shortage of literature connected to quantifying the effect of diffuser fouling, some aspects can be assumed. The material build-up in addition to the displacement thickness from the boundary layer result in a reduction in the effective cross-sectional area of the diffuser. In the book "Compressor Aerodynamics" by N. A. Cumpsty [35], the effect of narrowing of a clean radial diffuser channel is discussed. The narrowing of the diffuser channel increase in the radial velocity while having little influence on tangential velocity through the diffuser. This results in a shorter flow path through the diffuser. For a clean compressor this equates to a lower exit static pressure as less of the tangential velocity component is converted to pressure energy but a higher exit stagnation pressure due to lower frictional losses resulting from the shorter flow path. How this effect couples with increased roughness was however not covered, although it is fair to assume that both the static and the stagnation pressure will decrease compared to a smooth case.

One of the design parameters for diffusers is the length-to-width ratio which will be increased during fouling. For low values the diffuser tends to exhibit rotating stall while high values are dominated by increased friction losses. The length-to-width ratio is an important parameter when dimensioning the diffuser for the impeller section. Changes to

this ratio will create a mismatch between the components of the system resulting in increased losses. This as well as the findings of Haq and Bu-Hazza [30] highlight that the effect of fouling is not only limited to the region of material build-up but has an impact on components both upstream and downstream of the fouled component.

3.5 Fouling Correction Models

How the effect of changes in the Reynolds number influence the performance of turbomachines is well covered in literature. Sturb et al. [36] introduced a method with the aim to correct for the efficiency, head and flow between a workshop test condition and a specified operating condition for centrifugal compressors. This method, from now on refer to as the “ICCAM procedure”, has been experimentally verified and is adopted in both the ASME PTC-10 [11] and ISO 5389 standards [12].

Syverud and Bakken [37] presented a modified version of the ICCAM procedure, from now on refer to as “roughness method”, where changes in surface roughness between the workshop and specified condition are computed in the same way as for changes in the Reynolds number. Similarly, to the ICCAM procedure, the roughness method includes correction for efficiency, flow and head coefficients, which will be presented below. All the ratios presented in the roughness correction equations below are, similarly to the ICCAM procedure, obtained at BEP where the ratio between the two scenarios are assumed constant for all operational points. The method only corrects for the Reynold dependent losses and is calculated for an operating point near BEP. Near BEP the portion of the Reynold independent losses, α_{Re} , can be assumed constant with a value of 0.3 [36]. Both methods operate with an average Reynolds number and relative roughness obtained from the impeller and diffuser section. Where the average Reynolds number is given by Equation 3.1. Luca Scarbolo et al. [38] proposed that the relative roughness of the ICCAM procedure should be obtained by a weighted average rather than a mean between the two components.

$$Re = \frac{\bar{U}d_h}{\nu_1} \quad (3.1)$$

The average velocity through the compressor section, \bar{U} , is approximated by $U_2/2$ and the hydraulic diameter, d_h by twice the impeller outlet tip width, b_2 .

Efficiency, flow and head correction

A visualization of the roughness method can be seen in Figure 3.7. The method relates the fouled condition to a clean specified point at a lower Reynolds number. This is done as the ICCAM procedure requires equal roughness for the test, specified and critical condition as seen by the green line in Figure 3.7. In the figure and the equations below, the subscripts cr, sp and test denote the critical, specified and test conditions, respectively. The friction factor of the fouled condition is calculated using Equation 3.2 where the Reynolds number is equal to the clean test condition and the roughness is that of the fouled condition. The fouled friction factor is then related to the clean specified point. This is done by a reduction in Reynolds number for the clean roughness by keeping the fouled friction factor and inserting the clean roughness in Equation 3.2. The clean critical value is obtained from the same equation using the clean roughness at a Reynolds number above critical condition. It is important to point out that a critical Reynolds number refers to the values at which the friction factor becomes asymptotic and not the transition from laminar to turbulent flow. When the friction factors are known the efficiency correction can be computed from Equation 3.3. The head and flow coefficient are found from Equations 3.4 and 3.5 for near BEP.

$$\lambda = \left(-1.8 \log \left[\frac{6.9}{Re} + \left(\frac{\left(\frac{e}{d_h} \right)^{1.11}}{3.7} \right) \right] \right)^{-2} \quad (3.2)$$

$$\frac{1 - \eta_{fouled,sp}}{1 - \eta_{clean,test}} = \frac{\alpha_{Re} + (1 - \alpha_{Re}) \left(\frac{\lambda_{fouled,sp}}{\lambda_{clean,cr}} \right)}{\alpha_{Re} + (1 - \alpha_{Re}) \left(\frac{\lambda_{clean,test}}{\lambda_{clean,cr}} \right)} \quad (3.3)$$

$$\frac{\psi_{clean}}{\psi_{fouled}} = 0.5 + 0.5 \frac{\eta_{clean}}{\eta_{fouled}} \quad (3.4)$$

$$\frac{\phi_{clean}}{\phi_{fouled}} = \left(\frac{\psi_{clean}}{\psi_{fouled}} \right)^{0.5} \quad (3.5)$$

As a roughness increase equates to a reduction in the specified Reynolds number, care should be taken when adopting this method. The domain of application of the ICCAM procedure seen in Figure 3.8 will be governing as it lays the foundation for the roughness correction. Haugen and Paulsen [3] tested the roughness correction towards their experimental results. They found that the correction did not produce satisfactory results as it either over or underpredicted the performance degradation. The assumption of constant ratio for the degradation did not match with the experimental results as the relative change

in Figure 3.6 was seen to increase for higher flow rates. This highlights the need for new reliable and efficient fouling correction models.

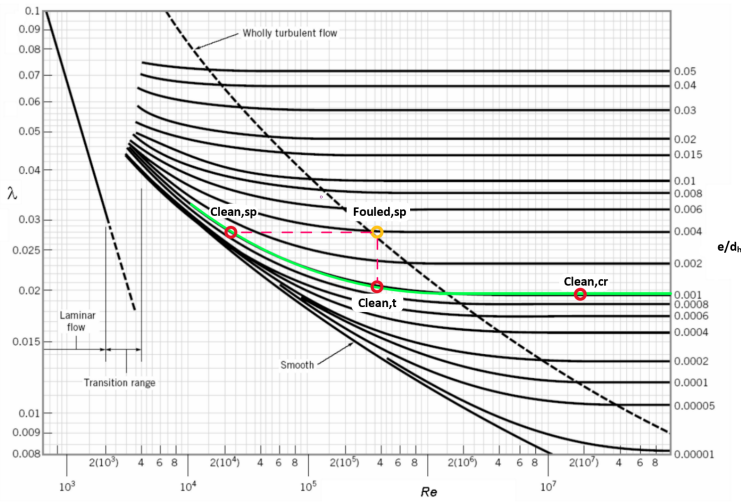


Figure 3.7: A visual representation of friction correction method given in [37].

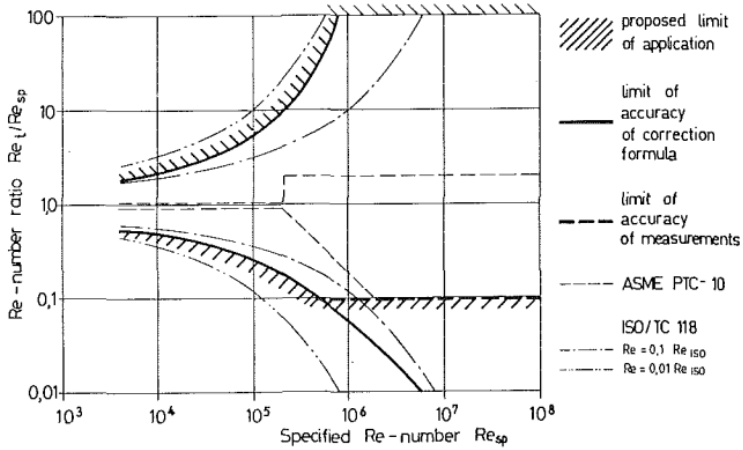


Figure 3.8: A visual representation of the application domain for the Reynolds correction method [36].

3.6 Summary

In this chapter different fouling mechanisms have been presented. The dominant entrainment mechanisms are turbulent diffusion for smaller particles and inertial impaction for larger ones. The material build-up is primarily dominated by process material polymerizing and adhering to the compressor surfaces. Parameters affecting the fouling rate are temperature, pressure, surface finish as well as gas composition. Compressor fouling changes the aerodynamic shape of the compressor components as well as the flow velocity, flow angles and surface roughness. The changes create a mismatch between the different compressor components. This allows for fouled area to impact both up- and downstream components. Despite substantial mass transfer to the pressure side of the impeller blades, rotating components are less likely to foul than stationary components due to centrifugal and dislodging forces. Condensate in the process stream was found to aid the fouling process for small amount while cleaning the compressor internals for larger liquid contents. A reduction in pressure ratio and polytropic head and efficiency was observed for the reviewed components when fouled. The reduction in compressor performance was found to be greatest for higher flow rates. Lowering of the GMF further reduced the performance with the greatest reduction for higher flow rates.

Fouling replication

In order to investigate the effect of diffuser fouling for both dry and wet gas scenarios, the diffuser section of the compressor rig (described in detail in Chapter 5.1) had to be coated with a fouling replica. The aim was to imitate the material buildup and increased roughness occurring during compressor fouling. It was essential that the selected replica could withstand the abrasive forces applied during dry and especially wet gas compression tests. Despite needing to be durable it was a requirement that the applied replica could be removed without causing damage to the compressor. Additionally it was required that the adopted fouling replica could imitate attributes of diffuser fouling found in industry. Figure 4.1 depict a severely fouled diffuser hub of the last stage of a retired multistage compressor, which served as a good comparative reference throughout the fouling replication campaign. In the following chapter attributes of diffuser fouling, reviewed methods and the adopted replication method, in addition to the application and removal process will be presented.



Figure 4.1: Fouled last stage diffuser hub of retired multistage compressor previously operating at Åsgard - now located at the NTNU wet gas compression facility.

4.1 Attributes of Fouling Material

It was important that the fouling attributes, roughness and thickness, were representative to that found in industry. Deposit samples collected from a hydrocarbon compressor at the research facility at K-lab can be seen in Figure 4.2. It is evident that there is a significant difference in both the deposit thickness from stage to stage but also within the same stage. It can be seen that the 1st diffuser stage has a thickness of 0.1 mm whereas the 2nd diffuser stage has a thickness that varies from 0.7-1.4 mm. The 2nd stage did also display a significantly rougher texture than the 1st stage diffuser deposits. The roughness of the deposits were obtained by Paulsen and Haugen [3] and found to have an equivalent sand grain roughness of 29-1015 μm . The adopted fouling replica was chosen to imitate the thicker and rougher side of the diffuser fouling spectrum. This was done in order to secure significant changes to the compressor performance as only one fouling scenario would be tested in the experimental campaign resulting from the Covid-19 time restrictions.



Figure 4.2: Deposits collected from different components of a hydrocarbon compressor at K-lab. The different samples, from left to right, were obtained from respectively: the U-bend, 1st stage diffuser, and two locations of the 2nd stage diffuser. The thickness of the deposits from the different compressor parts are highlighted in yellow.

4.2 Reviewed Materials

Haugen and Paulsen [3] investigated different fouling replication methods for wet gas compression with focus on removal and application procedures, durability and roughness. The materials investigated and their performance as fouling replicas are here shortly summarized. For a more in depth review, the reader is referred to [3].

Epoxy mixture: It was deemed not suitable for fouling replication due to tedious and time-consuming removal process. In addition to this, the epoxy mixture produced a smooth surface finish not desirable for fouling replication.

Texturized paint: Several types of paints were tested, and it was concluded that metallic paint was best suited to withstand the abrasive forces of wet gas compression. The texturization was obtained by introducing Plexiglas particles to the paint prior to the application. Plexiglas was chosen in order to prevent damages to the compressor internals when removing the paint or dislodgment of particles during compressor testing. The texturized paint was easily removed using paint remover.

Emery cloth: By changing the grit size of the emery cloth it was possible to obtain different and consistent roughnesses. The emery cloth would be super glued to a sheet of double-sided tape that would be super glued to the compressor part. The thickness could be regulated by the amount of double-sided tape sheets beneath the emery cloth. The cloth did not display good durability towards inertial impaction of liquid particles and had to be strengthened by epoxy mixture at the critical areas. The removal process of the replica using non damaging tools was tedious and time consuming. The most efficient solution was submerging the compressor part in a 90°C ultrasonic water bath.

For their inducer fouling tests, Paulsen and Haugen adopted the emery cloth replication method. Despite producing great results for the inducer fouling experiment, emery cloth was not be adopted as the fouling medium for the diffuser section. As submerging the diffuser section in a ultrasonic water bath to remove traces of the replica would not be possible, the removal process would be too time consuming. In addition, the emery cloth would be prone to dislodgement due to the tangential flow in the diffuser. A durability test was performed where the emery cloth replica was subjected to a power washer. The flow was tangential to the fouled plate to simulate the flow in the diffuser. The result backed the suspicion of the replica being peeled of as it took only 15 seconds for it to detach. Before and after pictures can be seen in Figure 4.3.

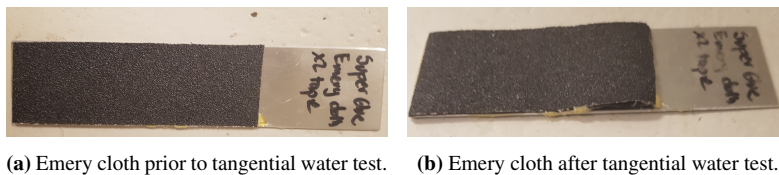


Figure 4.3: Emery cloth fouling replication before and prior to power washer stream test.

4.3 Metallic Texturized Paint

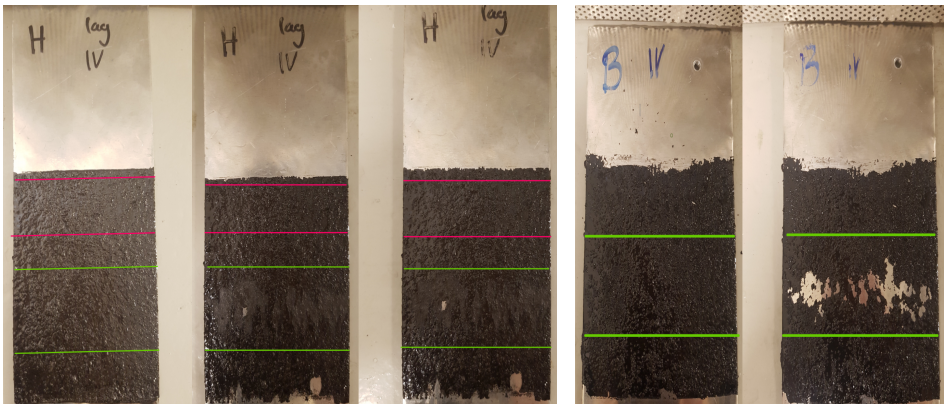
For this master's thesis, texturized metallic paint was chosen as the fouling replica. Fouling replications using paint have previously been done for axial compressors by both [39] and [40]. To the author's knowledge this has never before been done for centrifugal wet gas compression. Before any application to the diffuser section could start, validation of the durability, the application and removal procedure as well as the optimization of particle production, had to be performed. In addition to the metallic paint tested by Haugen and Paulsen ("Hammerite" [41]), another metallic paint, "Bengalack" [42], was tested to see if it displayed better properties.

4.3.1 Durability

In order to test the durability, test plates with 4 coatings of the different texturized paints were subjected to a power washer stream. For each of the test plates, two tests were scheduled. One with the power washer stream being tangential to the plate and one where the stream had a roughly 60° angle to the plate. Despite the flow in the diffuser being dominated in the tangential direction, water droplets can impact the hub side at inner radiuses at an angle [26]. The power washer nozzle was kept roughly 15 cm away from the test plate during the 5-minute test period for both the horizontal and normal tests. The results from the tests can be seen in Figure 4.4a and 4.4b where the green zone marks the 60° angle tests and the pink indicate the tangential test zone. From Figure 4.4a it is evident that there is some material loss from the 60° angle test. Apart from the spot where all the paint had been removed, the damage was inspected to only be the top two coating layers. For the tangential test there was not observed any damage to the coating. The Bengalack test plate was only subjected to 60° test as there was no point in performing the tangential test after it yielded significantly worse results than that of the Hammerite. As a result, Hammerite became the chosen metallic paint for the diffuser fouling replication. The bottom section of the Hammerite test plate and top section of the Bengalack test plate was subjected to tangential flow to inspect the effect of the water prying under the paint. As seen from in Figures 4.4a and 4.4b, significant damage was inflicted. Edges of the paint should thus be shielded from direct wet gas flow or reinforced.

4.3.2 Plexiglas Particles

Several methods were tested to produce the Plexiglas particles. The best result was obtained by collecting the Plexiglas shavings from processing it with a lathe. The thickness of the shavings was optimized to be 0.2 mm thick. It was found that thicker shavings were more difficult to break apart to smaller particles while thinner shavings would build to little texture and lump together during application. The final particles used in the coating would be obtained by crushing the shavings in two rounds to obtain a desirable and consistent size. The size of the unprocessed shavings as well as the two size reduction stages can be



(a) Hammerite test plate at different test stages: untested, 60° tested and tangential tested from left to right respectively.

(b) Bengalack test plate at different test stages: prior and after 60° test from left to right respectively.

Figure 4.4: Obtained results from durability tests for the Hammerite and Bengalack coated test plates.

seen in Figure 4.5. The obtained particles were mixed together with the metallic paint in a 1:4 volume ratio to obtain the texturized paint.



Figure 4.5: Sizes of the Plexiglas particles with with a caliper as reference. The unprocessed shavings is seen to the right, the first size reduction in the middle and the final reduction step to the left.

4.4 Diffuser Fouling Replication

Despite fouling in the diffuser section being observed on both the hub and shroud side in both literature and observation of the fouled in-house compressor in Figure 4.1, the texturized paint was only applied to the hub side of the diffuser. This was done due to restrictions set by the supervisor discussed in Section 1.3. The effect of increased roughness and reduced flow area resulting from diffuser fouling was still possible to replicate even if the fouling replica is only applied to the hub diffuser wall.

Despite the texturized paint displaying a good durability towards the inertial impaction of the water in the durability tests, visual confirmation of the state of the fouling replica was of great importance. In order for the different fouling tests to be comparable to each other, the state of the coating had to be comparable for the different tests. In order to easily observe damages to the coating, the different layers were applied with different colors. This allowed for easy validation of the state of the coating prior, during and after the tests and which tests were performed with comparable fouling.

Only fouling one side of the diffuser will change the velocity profile within the diffuser. Bakken and Bjørge [43] investigated the effect of backflow from the volute section during wet gas compression. It was observed that the backflow caused hysteresis as the volute flow would change direction at different volume flows when either going from high to low or low to high flow rates. It was unknown how velocity profile changes resulting from fouling would interact with this effect. Visual confirmation of the flow regime was thus of great importance. In order to prevent the hysteresis impacting the experimental campaign, all wet gas tests should be performed with descending flow rates.

4.5 Application and Removal Procedure

Application

Prior to initiating the fouling tests fouling of the diffuser section had to be conducted. The coats of texturized paint were applied with the use of brushes. Struder et al.[39] replicated axial compressor fouling by applying paint to the impeller blades. Emphasis was put on having spanwise brush strokes to ensure uniform thickness. For the application of texturized paint to the diffuser section focus was directed towards dispersing the Plexiglas particles to preventing them lumping together. Despite trying to maintain a uniform thickness, the vertical application resulted in gravity affecting its uniformity. Due to the random nature of diffuser fouling, there is no such thing as a uniform fouling thickness which can be easily seen in Figure 4.1.

A total of 11 coats of texturized paint were applied to the back-diffuser wall. The thickness of the applied coating was measured upon removal and was found to vary between 1.6 and 2.2 mm (excluding particles extending outside the base layer), with an average of 2mm.

A visualization of the diffuser section before and after applying the fouling replica as well as a cross sectional view of the thickness can be seen in Figures 4.6a-c. As stated in the previous section, the coating layers alternated their colors. The three outermost layers had the following sequence starting from the top: silver, black and red.

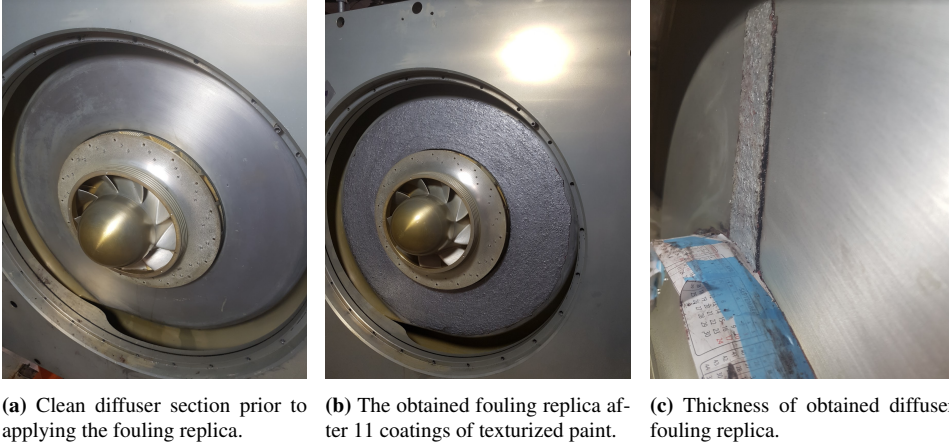


Figure 4.6: A visual of the hub side of the diffuser prior and after the fouling replication procedure in addition to a cross sectional view of the applied coating.

As mentioned in Section 4.3.1 the texturized paint suffered when the power washer stream was able to dig underneath the applied coating. To prevent the flow exiting the impeller from digging under the applied coating, the edge of the coating was extended to the clearance gap between the impeller and diffuser. In Figure 4.7 the clearance gap is marked with a green circle and the fouling replica illustrated in red. In order to roughen the somewhat smooth paint surface, emery cloth was pressed against the final layer halfway through its drying process. The new roughness felt similar by touch to that seen in Figure 4.1. The surface finish of the final layer before and after the roughening process can be seen in Figure 4.8

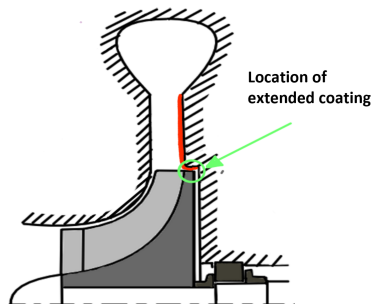


Figure 4.7: Visualization of the extended coating obtained to prevent flow digging under the fouling replica.

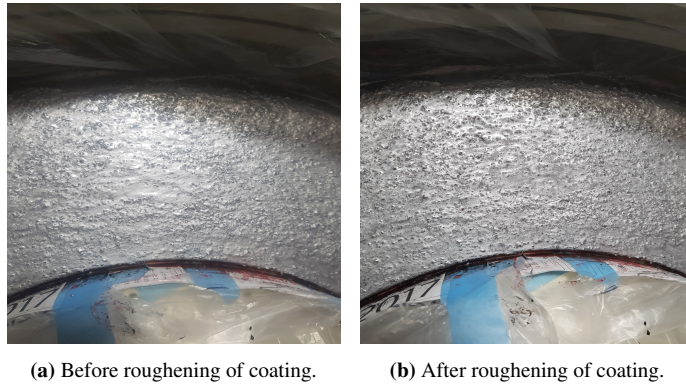


Figure 4.8: Surface finish of of the final coating layer before and after roughening with emery cloth.

Removal

After the conducted fouling tests the coating was removed. Initially paint remover was applied to the top layer in order to remove it by a flat wide Plexiglas scraper. The paint remover only affected the top layer and this method proved to be very time-consuming. To speed up the process a different scraper was created by cutting a 1x5x20cm Plexiglas plate at a 45° angle. The new scraper design resulted in a smaller surface area contacting the paint and thus focusing the applied force. This allowed for several layers to be removed at the same time in 1cm wide strips. The adoption of the new scraper resulted in a significant time reduction of the removal process. The remaining coating was removed by applying paint remover. A visual of the diffuser section during and after the removal process can be seen in Figure 4.9. No damages to the diffuser section or other components resulting from testing or the removal process was observed when examining the cleaned compressor.

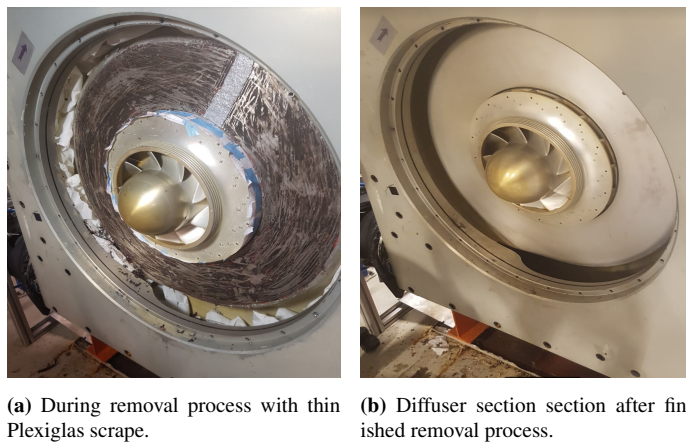


Figure 4.9: Diffuser section during and after removal of texturized paint.

4.6 Summary

In this chapter different fouling replication strategies have been presented. Metallic paint containing Plexiglas particles in a volume fraction of 4:1 was chosen as the fouling replica for the diffuser section. Durability tests in addition to application and removal procedure for the adopted fouling replication have been presented. The fouling of the diffuser section have only performed on the hub side of the diffuser due to restrictions regarding the Plexiglas diffuser shroud. A total of 11 coats were applied resulting in an average thickness of 2 mm. The thickness was comparable to twice the thickness of fouling samples gathered from K-lab, thus being representative of the total width reduction.

Chapter 5

Experimental Campaign

In this chapter the present NTNU wet gas compression test facility will be presented. The overall objectives of the experimental campaign, the laboratory test procedure, data processing and uncertainties will also be presented.

5.1 The NTNU Wet Gas Compressor Test Facility

The wet gas compression test facility at NTNU aims to enhance the in-depth knowledge regarding wet gas compression. The test facility was made in collaboration with industry partners and contributes to industry as well as academic research. Over the years, the compressor has been subjected to several changes and is frequently modified in order to satisfy the needs of ongoing master's and doctoral thesis' in addition to industry projects. The compressor rig seen in Figure 5.1 consists of a single stage centrifugal compressor with backswept impeller blades and vaneless diffuser. The compressor operates in an open loop configuration with a low inlet pressure. For the wet gas compression, air and water is used as the working fluids. Despite the difference in operational parameters, low pressure air-water compression has proven its ability to successfully predict the performance trends for high pressure hydrocarbon wet gas compression [44].

Air is drawn into the system and passes through an orifice flowmeter. The mass flow of the air is computed from the orifice measurements in compliance with ISO 5167-2 [45]. The flow rate of air in the system is regulated by a throttle valve downstream of the compressor. The introduction of water is regulated by a liquid injection module with spray nozzles that can be adjusted independently. The active nozzles and their configuration are chosen based on the water demand for the different GMFs while still maintaining a uniform water-spray at the compressor inlet. Whereas a GMF=0.99 only needed one of the smallest nozzles

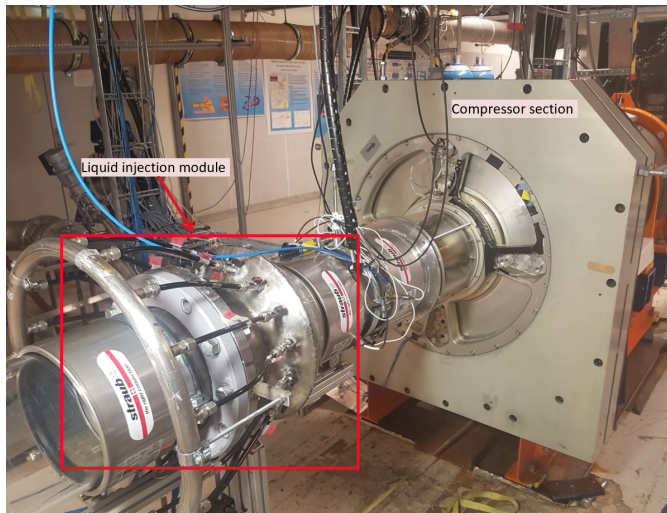


Figure 5.1: NTNU wet gas compressor displaying the liquid injection module.

(NF01), $GMF=0.80$ required all nozzles (both NF01 and NF06) to produce the required GMF. Information relate to the different nozzle sizes and their operating ranges can be found in [46]. A representation of the nozzle layout in the water injection module can be seen in Figure 5.2.

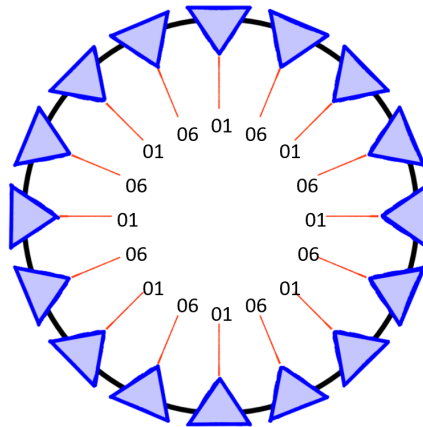


Figure 5.2: Nozzle layout of water injection module.

The complexity of multiphase flow is eased by a visual confirmation of the flow pattern both entering and through the compressor. To obtain a visual of the flow regime, the wet gas compressor at NTNU is installed with Plexiglas at the impeller inlet, as well as at the frontal diffuser wall and volute section. The importance and benefits of the

transparency of the Plexiglas have already been mentioned in Section 4.4. The introduction of Plexiglas and corresponding seals does however limit the allowable maximum pressure in the compressor system.

The compressor is driven by an electric motor (450 kW) and controlled through the usage of a variable speed drive unit. The impeller is fixed to the driver shaft of a bearing pedestal in order to prevent water damage in the electrical motor during wet gas testing. The bearing pedestal is connected to the electrical motor through a torque meter, in order to accurately measure the static and dynamic compressor power.

The data acquisition system used at the facility is the National Instruments PXI solution, which permits synchronous sampling up to 20 kHz. The compressor setup and instrumentation are in accordance with ASME PTC-10, at dry gas conditions [44]. A P&ID of the compression facility is visualized in Figure 5.3, showing the sensors and instrumentation used in addition to their respective accuracy. The main dimensions and operating range and conditions for the compressor setup is given in Table 5.1. For a more in-depth description of NTNU wet gas compressor test facility, the reader is referred to "Integrated Wet Gas Compressor Test Facility," by Hundseid and Bakken [47]

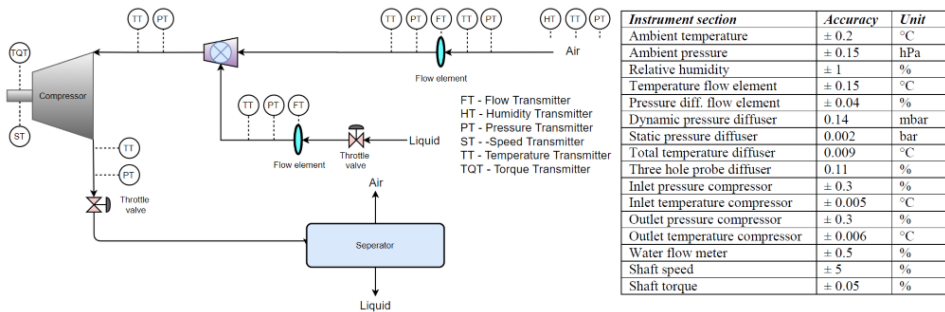


Figure 5.3: Test rig P&ID with corresponding test rig instrumentation and accuracy [47].

Table 5.1: Main dimensions and operating ranges of NTNU wet gas compressor setup [47].

Main Dimensions and Operating Ranges	
Impeller outer diameter (D_2)	40mm
Diffuser width (b)	20mm
Diffuser ratio (D_3/D_2)	1.7
Inlet hub diameter	250mm
Outlet pipe diameter	200mm
Suction conditions	Atmospheric
Test fluids	Air/water
Air-flow range	0-3 kg/s
Water-flow range	0-5 kg/s
GVF range	99.93-100 %
GMF range	40-100 %
Electric motor	Max: 450kW & 11 000 RPM

5.2 Objectives

In accordance with the scope of this master thesis, the experimental campaign will be conducted to complete the following objectives.

- Establish relevant compressor performance characteristics for unfouled case for both dry and wet gas scenarios to serve as references for the fouled tests.
- Test and document how fouling of the diffuser section affects and alters the dry and wet performance characteristics.
- Document the durability of adopted fouling replication. The location and severity of the potential wear shall be investigated both during and after fouling tests.

5.3 Test Campaign

Initially the test campaign would test four different fouling coatings with two different thicknesses and two different roughnesses. This was suggested in order to better quantify the change in compressor performance with respect to changes in diffuser width and roughness. Due to COVID-19 and lockdown of the NTNU test facility, the test period was severely reduced and changes had to be made. Only one coating with its respective roughness was tested within the available time frame. Both fouled and unfouled tests was subjected to different GMF's in order to visualize the change in performance with varying liquid content. Initially, only the GMFs (1, 0.975 and 0.90) tested by Haugen and Paulsen [3] were to be tested to better compare the effect of fouling in the diffuser and inducer section. The fouling replica displayed great resistance towards the abrasive forces of the flow, and additional GMFs were tested. The GMFs 0.99 and 0.80 were tested to better observe the effect of fouling on a broader part of the wet gas operational domain.

5.3.1 Logging of Operational Parameters

In order to measure the effect fouling has on the diffuser section, several operational parameters had to be measured for the different test conditions. The operational parameters for the different tests were, in accordance with ISO 5389 [12], taken close to steady state values. This was done in order to reliably compare with other obtained values. When operating the compressor during dry gas testing, the temperature of the ambient air in the compressor lab as well as the piping, compressor and other equipment will increase. Achieving steady state for the different dry gas operating points would thus require substantial run time and was therefore deemed not feasible for this master thesis. A "semi steady state" (SSS) was adopted instead. The operating parameters would achieve SSS when the measured values did not vary outside of the uncertainty limit of the measuring device over a 10-minute period. The obtained SSS value was obtained by averaging the logged values from the last 60 seconds for the measured operating point. The operational parameters will be logged by the instrumentation presented in Figure 5.3.

During wet gas compression test, the inlet and exit temperature measurements fluctuated due to liquid covering the measuring probe resulting in wet bulb temperature readings. This rendered the temperature readings useless. To overcome this problem and reliably predict the compressor performance in wet gas scenarios, accurate measurements of the shaft torque was of great importance. The water temperature in addition to the ambient air temperature at the air intake were used to compute the compressor inlet temperature in HYSYS¹. By utilizing the shaft torque instead of the outlet temperature measurements, substantial time savings could be made as thermal stability was not needed at the compressor discharge. Tests utilizing both discharge temperature and shaft torque for dry gas conditions were compared and yielded similar results. Thus further time savings could be made by adopting the shaft torque for the dry gas tests. This reduced the test time of the different operational points for dry gas from 1 hour to 30 minutes.

In order to establish the performance characteristics for the different tests, five operational points were logged. As all the tests would yield new performance characteristics, both the surge line and the choke line had to be established. The operational points (OP) that will be logged are: OP1 near surge, OP3: on (or near) BEP, OP2: Between OP1 and OP3, OP:4 between BEP and max flow, and OP5: max flow. The operational points were determined from prior dry gas compression tests and relate to specific openings of the discharge valve. The operational points and their respective discharge valve opening can be seen in Table 5.2.

Table 5.2: Operational test points at 9000 RPM with corresponding discharge valve openings.

Operational Point	Discharge Valve Opening
OP1 (near surge)	30%
OP2	42%
OP3 (BEP)	54%
OP4	75%
OP5 (max flow)	100%

5.3.2 Fouled Diffuser Test

Initially only the GMFs 1, 0.975 and 0.9 were proposed to be tested. Despite performing durability tests on the texturized paint there was some uncertainty connected to how long the coating would resist the compressor flow. The tests were therefore performed with descending GMFs to conduct the experiments with gradually increasing load to the coating. The instrumentation for the wet gas tests were identical to the one used for dry gas although no wet gas test protocol equivalent to the ASME PTC-10 [11] exists. Signs of wear in the coating were checked between operational points and tests. No signs of damage to the coating were observed during or after the initial tests which permitted for testing of the GMFs 0.99 and 0.80. The test matrix for the diffuser fouling tests can be seen in Table 5.3.

¹A computational tool provided by AspenTech which allows for compressor calculations

Table 5.3: Test matrix for the fouled diffuser tests for dry and wet gas compression.

Compressor speed [RPM]	GMF [-]	Operational point	Roughness	Coating thickness
9000	1	OP1	Rough	2 mm
	0.99	OP2		
	0.975	OP3		
	0.90	OP4		
	0.80	OP5		

5.3.3 Unfouled Baseline Tests

After the paint had been removed from the diffuser section unfouled compression test could be conducted. In order to document the changes in the compressor performance resulting from diffuser fouling, unfouled performance tests for dry and wet gas compression were carried out. These performance tests served as comparable references for the already conducted fouled performance tests. The test matrix for the clean baseline tests can be seen in Table 5.4.

Table 5.4: Test matrix for the fouled diffuser tests for dry and wet gas compression.

Compressor speed [RPM]	GMF [-]	Operational point	Roughness	Coating thickness
9000	1	OP1	Smooth	No thickness
	0.99	OP2		
	0.975	OP3		
	0.90	OP4		
	0.80	OP5		

5.3.4 Test Procedure

The test matrices given in Tables 5.3 and 5.4 followed the test procedure for dry and wet gas given below.

Dry gas performance tests

0. If the test is the first test of the day, perform a still test to validate the recorded values of the measuring instrumentation. This will be used for post-processing of the logged values.
1. Follow start-up procedure given by NTNU compressor lab.
2. Accelerate rotational speed to 9000 RMP with discharge throttle valve at 30% opening in order to faster heat up the piping and compressor. Let the compressor run for 20 minutes and start a 10-minute logging of OP1.

3. Open the discharge throttle valve incrementally in order to log the operational points given in the respective test matrices, from low to high flow rates. Before logging each point for 10 minutes a 20 minute stabilisation period shall be performed for each point. All values should be obtained at semi steady state.
4. After logging all points, initiate compressor shut down procedure for NTNU compressor lab testing.

Wet gas performance tests

Wet gas tests

1. Follow dry gas start-up procedure point 0 and 1.
2. Accelerate rotational speed to 9000 RMP with discharge throttle valve fully open.
3. Adjust the water flow to match the appropriate GMF by either changing the active nozzles or adjusting the water throttle valve.
4.
 - (a) If the coating is prone to significant wear as a result of liquid introduction, the logging will be prioritized for OP5, OP3 and OP1 in order to produce some results for the different GMFs. Afterwards OP 4 and OP2 will be logged to fill out the performance curves.
 - (b) If the coating displays satisfactory wear resistance, logging will be conducted by going from OP5 to OP1.
5. Between each operational point, liquid content shall be reduced to zero in order to visually inspect that no significant damage has been inflicted on the coating. Step 3 will have to be deployed before next point can be logged.
6. After all points have been logged, reduce the water flow to zero and let compressor run dry.
7. Initiate compressor shut down procedure for NTNU compressor lab testing.

5.3.5 Data Processing

Prior to analyzing the obtained SSS values from the different compressor tests, the respective still test measurements were studied. The obtained values from the different pressure and temperature sensors, in the locations where more than one were present, were compared to each other to validate the readings. In addition, the static torque reading was logged. The obtained offset for the different sensors were then utilized as a static correction for the respective performance tests.

The measured values from both the still tests and performance tests were analyzed and extracted from DIAdem². The obtained SSS value where several measuring probes were present was taken as the average value. The only exception was for wet gas compression where one of the four pressure sensors at the inlet would be covered by water due to it being located at the bottom of the pipe. This resulted in it measuring the water column on top in addition to the inlet pressure and was consequently removed from the averaging.

Not all the properties needed to compute the compressor performance could be directly measured and had to be calculated from other obtained values. The air mass flow was computed with Reynolds correction in accordance with ISO 5167-2. The inlet air volume flow was derived from the air mass flow rate and the GMF was calculated from the water and air mass flows.

The averaged semi steady state values were fed into HYSYS, yielding the polytropic head and polytropic efficiency. Soave-Redlich-Kwong was used as the equation of state as it is the preferred by NTNU/Equinor for wet gas compression containing air-water-mixture [48]. The steady state HYSYS model used in this master is presented and explained in “Appernix B- HYSYS Model”.

5.3.6 Experimental Uncertainties

Liquid injection module: The liquid injection module should be operated such that the flow regime and pattern are as consistent as possible, when varying the water flow for the different GMFs. Changes in either flow pattern or mean droplet size could be sources of uncertainty. As less water is required for a specific GMF at lower flow rates compared to higher, the flow pattern and size of the droplets will vary slightly for the different operational points. Although difficult to validate the droplet size, visual confirmation of annular flow for all operational points was important.

Fouling distribution and appearance: There is a lack of experimental data from the industry for wet gas compressor fouling. The distribution of fouling in the radial direction in the diffuser was not found in literature. As the texturized paint was applied to the vertical diffuser, the paint was affected by gravity. The fouling thickness was found slightly greatest at the outer radiuses for the bottom half of the diffuser. If the liquid is primarily introduced to one side of the impeller it may cause one part of the diffuser to be more exposed. If the changes in thickness and roughness differ in the different sections of the diffuser this may cause slightly varying results. Visual confirmation of the flow regime in the diffuser and maintaining a uniform flow in the radial direction was thus important for all operational points.

Air mass flow calculations: The initial relative humidity in the compressor lab will typically be in the range of 20-40%. As the compressor rig is an open loop, the pressurized

²A software from National Instruments designed to help engineers and scientists to quickly inspect, analyze and report on measured data

air-water-mix is dispersed into the air. This drastically changes the relative humidity in the room. The temperature and relative humidity affect the humid air density. Being able to accurately measure these values are essential in order to obtain a reliable computed value of the gas mass flow rate over the orifice.

Wet gas temperature and torque: The limits for allowable uncertainty are well described in ASME PTC-10 [11] for dry gas conditions. Currently there is no equivalent standard for wet gas compression. Temperature readings for wet gas compression are difficult and unreliable. As mentioned in Subsection 2.4.3, thermal equilibrium at the compressor exit is not expected owing to different heat capacities of the liquid and gas phase. This phenomena is not captured in HYSYS which calculates an equilibrium temperature at discharge. In addition, wet bulb temperature readings where liquid covers the temperature sensor can occur at both the compressor inlet and outlet. The NTNU wet gas facility utilizes a torque meter to account for the power input thus removing the need for outlet temperature readings. The compressor inlet temperature was obtained through HYSYS by equalizing the properties over the mixer. A more in depth explanation can be found in Appendix B - HYSYS Model. The air temperature used was from a temperature sensor located at the air intake. This temperature reading had been measured 0.5-1°C lower than the compressor inlet temperature during dry gas testing. A sensitivity study was performed to validate if the change in air temperature was significant for wet gas testing. The difference was found to alter the performance by only 0.2% for the efficiency and polytropic head. This method was thus preferred to utilizing the inlet temperature readings which fluctuated with several degrees Celsius due to liquid coverage.

Pressure readings: Computations of the compressor performance using the steady state HYSYS model is especially sensitive to the pressure at compressor inlet and discharge. Both the compressor inlet and exit have four pressure sensors to obtain accurate measurements. The sensors were calibrated using the offset from the respective still tests. Despite this the pressure sensors at the discharge diverged with a maximum of 0.6 kPa for lower flow rates. A sensitivity study was performed to see the effects of the deviation. The results showed a 2.7 % change in the obtained polytropic head and efficiency. As this phenomenon was consistent for all tests it was deemed important that the procedure was kept consistent throughout the test campaign to reduce the impact of the fluctuations. As none of the measured values were obvious to refute, the obtained discharge pressure was taken as an average for all tests. This contrasts with the inlet pressure where one of the pressure sensors were refuted due to being covered with water column. In order to have comparable pressure readings for wet and dry gas, the same pressure sensor was removed from the dry gas inlet averaging.

5.4 Summary

This chapter has presented the experimental campaign where a total of five GMFs ranging from 1 to 0.80 have been conducted for both clean and fouled conditions. The NTNU wet gas compression rig has been presented in detail, including instrumentation, main dimensions and operating ranges. The objectives of the experimental campaign were presented. The shift in compressor performance between clean and fouled operations, as well as the experimental performance of the fouling replica was to be documented. The logging method, test matrices and procedures, data processing and uncertainties has also been presented.

Chapter 6

Results and Discussion

Available knowledge on how fouling impacts the performance curves of centrifugal compressors is limited. The conducted test campaign presented in the previous chapter served to enhance the understanding of centrifugal compressors operations. The results obtained from the experimental test campaign will be presented and discussed in the following chapter.

The following chapter will be divided into two parts:

1. Performance characteristics
2. Experimental experience

6.1 Performance Characteristics

In the following section compressor performance characteristics for both dry and wet gas scenarios with and without diffuser fouling will be presented. The polytropic head and efficiency as well as pressure ratio curves will be normalized and plotted against the normalized suction volume flow rate. The normalization will be towards the values obtained from the BEP for the clean dry gas test. The performance characteristics were obtained by utilizing a third order polynomial regression curve to best fit the calculated values produced by the HYSYS calculations. In the plots the fouled and clean conditions are denoted by the letters, f and c, respectively.

6.1.1 Clean Baseline Performance

Polytropic Head

Figure 6.1 shows the polytropic head obtained from the HYSYS steady state model. A clear reduction in the polytropic head can be seen when lowering the GMF. The results concur well with the findings in [3] and [17]. The prominent reduction in polytropic head with increased liquid content can be helped explained by Equation 2.16. As the energy associated with pressurisation of water is substantially lower than that of air the polytropic head is reduced with decreasing GMF. In addition to this, increased losses further reduces the polytropic head. For the GMFs 0.90 and 0.80 the curves are slightly sloping downwards for low flow rates. This indicates the compressor experiencing surge which was confirmed by visual confirmation of a liquid doughnut at the compressor inlet during testing. The compressor operating domain is thus reduced as a result.

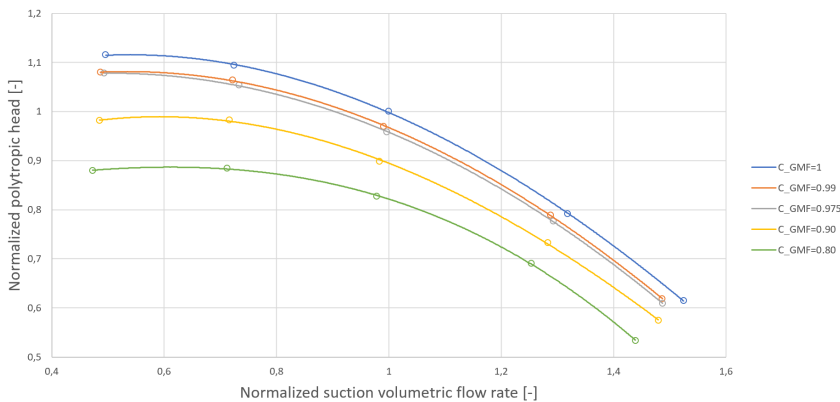


Figure 6.1: Normalized polytropic head curves for the tested GMFs at clean conditions.

Pressure Ratio

Figure 6.2 shows pressure ratio curves obtained from the unfouled baseline tests for the respective GMFs. From the obtained results it is clear that wet gas compression yields a higher pressure ratio compared to dry gas compression for around BEP to low flow rates which is linked to the increased flow density due to evaporative cooling and heat transfer [49]. The increase is seen not to vary significantly with respect to GMF. The difference in pressure is seen reduced for all GMFs for increasing flow rates. At max flow, the wet gas pressure ratio curves coincides with that of the dry gas. The reduction in the difference between the wet and dry gas pressure ratio at increasing flow rates is caused by increased losses for wet gas compression.

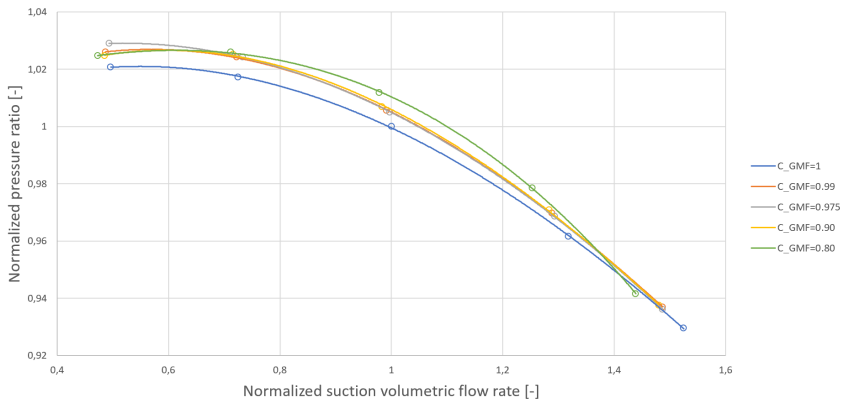


Figure 6.2: Normalized pressure ratio curves for the tested GMFs at clean conditions.

Efficiency

Figure 6.3 shows the normalized polytropic efficiency obtained from HYSYS for the different GMFs at unfouled condition. The measured power consumption for the wet gas compression tests was not proportional to the increase in total mass flow thus indicating increased losses. According to Hundseid et al. [14] increased friction and compressibility losses are the main contributors to the increased losses in wet gas compression. The increased losses reduce the efficiency of the compression process. The tendency of reduced efficiency with reduction in GMF is clearly visible in the plot. The location of the BEP, visualized as a solid colored circle, is shifted towards higher flow rates when going from GMF=1 to GMF=0.975. For the lower GMFs it can be observed that the BEP is shifted towards lower flow rates compared to GMF=1. This trend was also observed by Paulsen and Haugen [3].

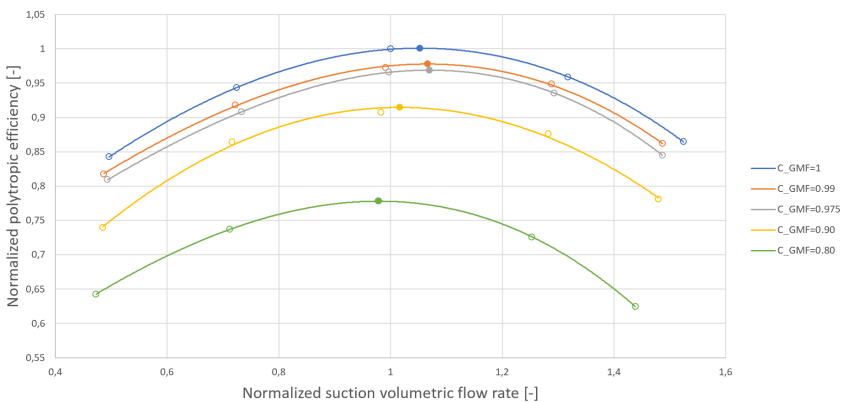


Figure 6.3: Normalized polytropic efficiency for tested GMFs at clean conditions.

Flow Throughput

From the previous figures one can observe a distinct reduction in the maximum flow throughput for descending GMFs resulting from the increased resistance in the system. The sharp reduction in maximum flow rate for GMF 0.99 and 0.975 is not consistent with that of [3] and [17] which display an almost linear reduction of the maximum throughput for decreasing GMFs as seen in Figure 2.6b. The sharp reduction may result from the inlet temperature produced by HYSYS being 2°C colder than the lowest recorded inlet temperature reading for the two highest wet gas GMFs. If [3] and [17] used the recorded inlet temperature values, it may explain the obtained difference. As the method of obtaining the inlet temperature is not specified in mentioned sources, it is impossible to say for certain. It is important to state that the recorded inlet temperature readings for GMF 0.99 and 0.975 differed with up to 5°C. The HYSYS inlet temperature was thus adopted instead of averaging the temperature readings in order to reduce the uncertainty. For the lower GMFs the computed temperature in HYSYS displayed a significantly lower difference with the recorded values which may explain their linear trend with respect to GMF=1.

6.1.2 Effect of Fouling on Polytropic Head

Dry gas

In Figure 6.4, the polytropic head for both fouled and clean conditions are plotted against the total volume flow rate. The reduction in polytropic head is seen to be prominent for the whole operational domain. Prior to the obtained results it was expected that the two curves would diverge more at higher flow rates as seen in Figure 3.4a owing to the increased frictional losses being dominant. The relatively constant reduction indicate that the degradation is heavily affected by blockage and shock losses. More detailed experiments are however needed to verify this. A reduction in the volumetric flow rate can be observed for the fouled case at max flow as a result of increase resistance in the system.

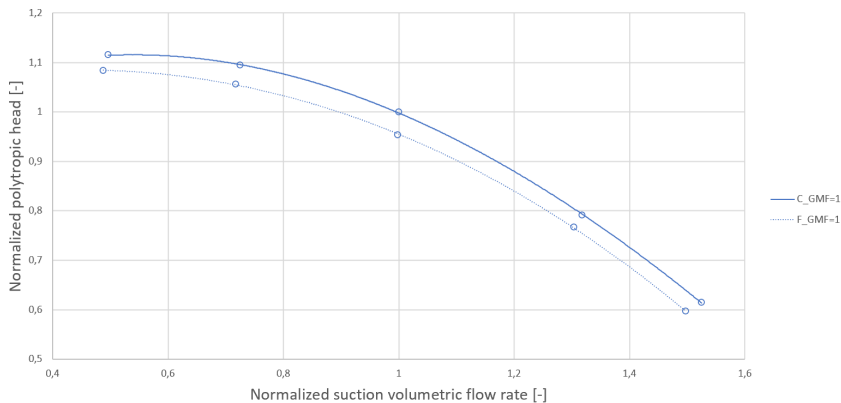


Figure 6.4: Normalized polytropic head curves for the clean and fouled dry gas compression tests.

Wet gas

Figure 6.5 display the polytropic head curves for GMF 0.99 and 0.975 for clean and fouled conditions. Similarly, to that of dry gas, the polytropic head is reduced for the fouled tests. However, the effect of the fouled and clean curves diverging at higher flow rates are more pronounced compared to GMF 1. Owing to the liquid's higher viscosity, the frictional losses are increased. There is not observed a substantial difference in the polytropic head reduction for the two different GMFs. This might indicate that despite the increased liquid content there is not a substantial increase in the amount of liquid interacting with the fouled hub diffuser side. Similarly to that of GMF=1, a reduction in the maximum throughput resulting from the fouling replica can be observed.

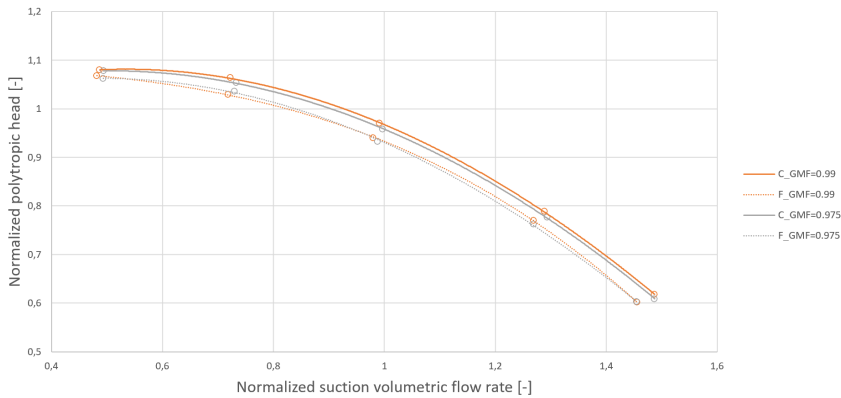


Figure 6.5: Normalized polytropic head curves for clean and fouled conditions for GMF 0.99 and 0.975.

Figure 6.6 display the polytropic head curves for GMF 0.90 and 0.80 for clean and fouled conditions. The twisting of the polytropic head curve can be seen more noticeable for the plotted GMFs. The steeper slope of the fouled curves can be seen to surpass the unfouled cases for lower flow rates instead of almost converging with the clean tests as seen for the higher GMFs. This can be explained by the clean compression tests for GMF 0.90 and 0.80 experienced light surge at these flow rates while the fouled conditions did not. The difference at low flow rates can be seen more pronounced for GMF=0.80.

6.1.3 Reduction in Polytropic Head Due to Fouling

In Figure 6.7 the reduction in polytropic head in percent when going from clean to fouled scenarios is plotted against the normalized volume flow rate at fouled conditions for the respective GMFs. The reduction curves of GMF 1, 0.99 and 0.90 exhibit steep slopes for both high and low flow rates with a flatter slope around OP3. The reduction curves of GMF 0.975 and 0.80 are more of an exponential nature with the slope being steepest at

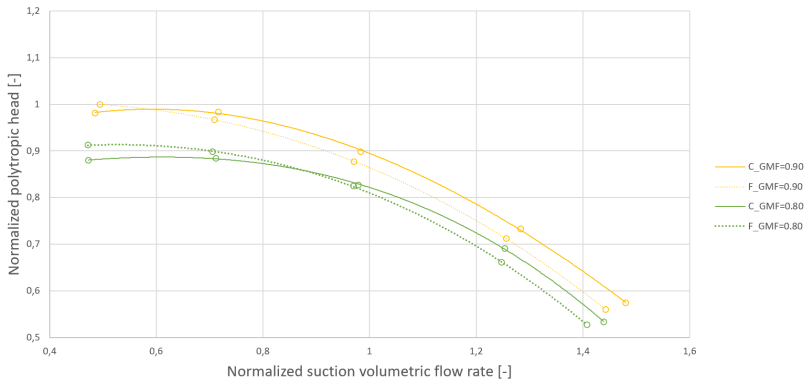


Figure 6.6: Normalized polytropic head curves for clean and fouled conditions for GMF 0.90 and 0.80.

max flow rate. Despite the different shape of the reduction curves, a clear tendency of a stronger reduction at high flow rates can be seen for all GMFs plotted. This tendency concurs well with the obtained results in [3]. Both GMF 0.90 and 0.80 display an increase in polytropic head at lower flow rates. In order to verify and further test the effect of percentage-wise reduction in polytropic head at higher flow rates, additional roughnesses should be tested.

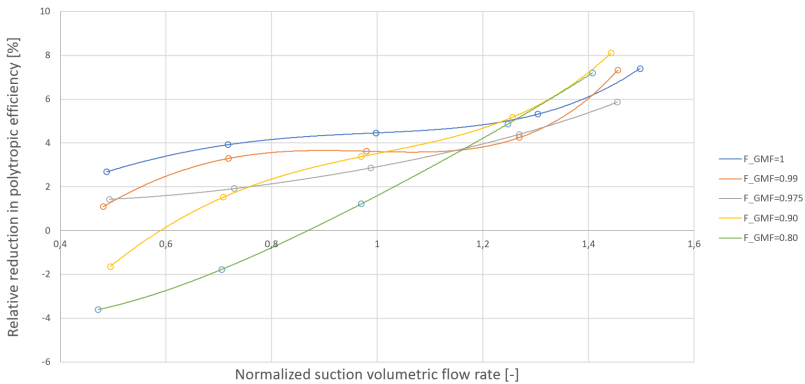


Figure 6.7: The relative reduction in polytropic head when going from clean to fouled scenarios for the tested GMFs.

6.1.4 Fouling Impact on Pressure Ratio

Dry gas

The normalized dry gas pressure ratio curves for clean and fouled conditions in Figure

6.8 display similar trends as the ones in Figure 6.4. The relationship between the pressure ratio and polytropic head using Schultz method is given by Equation 2.9

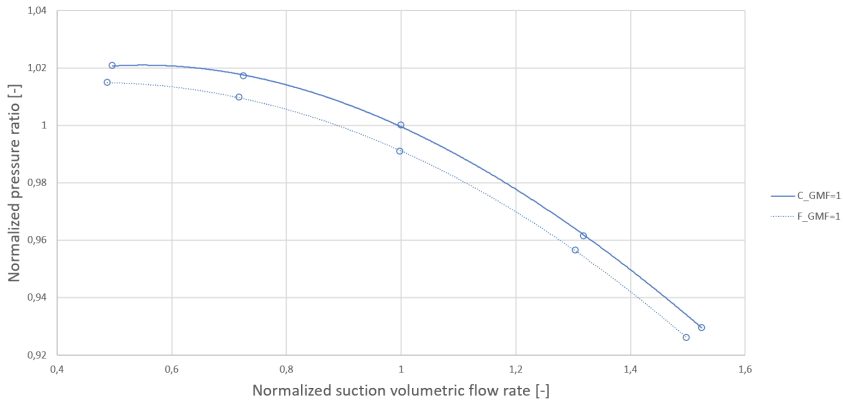


Figure 6.8: Normalized pressure ratio curves the for clean and fouled dry gas compression tests.

Wet gas

The wet gas pressure ratio curves at fouled and clean conditions for GMF 0.99 and 0.975 can be seen in Figure 6.9. A reduction in the pressure ratio can be observed when moving from clean to fouled conditions for both GMFs. The tendency of the two GMFs coinciding at higher flow rates is still present for the fouled conditions although the curves diverge more at lower flow rates compared to the clean scenario.

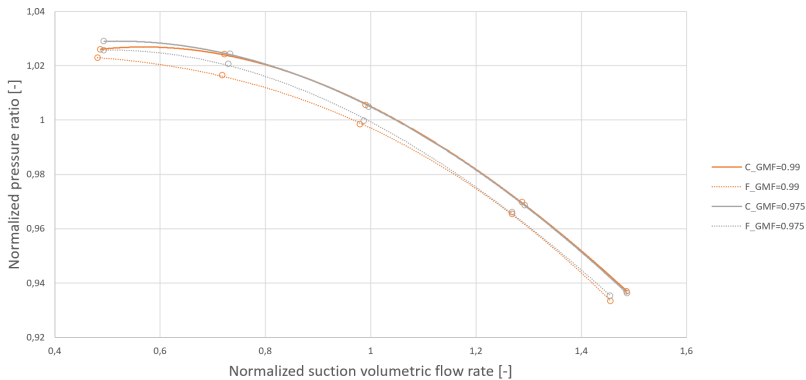


Figure 6.9: Normalized pressure ratio curves for clean and fouled conditions for GMF 0.99 and 0.975.

Figure 6.10 display the pressure ratio curves for GMF 0.90 and 0.80 for fouled and clean conditions. A reduction in the pressure ratio can be observed for both GMFs at higher flow rates. The pressure ratio is however higher for fouled conditions for both GMFs at lower

flow rates. The region where the fouled pressure ratio surpasses the clean condition is significantly larger for GMF 0.80 compared to GMF 0.90 as seen in the plot. In industrial applications where the compressor operates with a fixed outlet pressure, the reduction in pressure ratio due to fouling will restrict the allowable throughput of the compressor if no changes to inlet parameters or rotational speed are made.

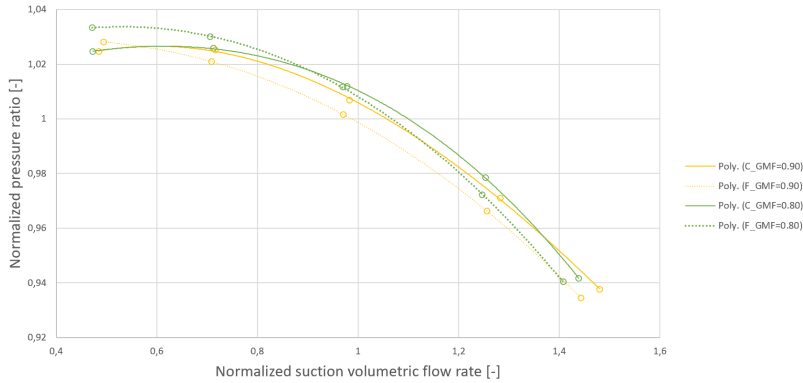


Figure 6.10: Normalized pressure ratio curves for clean and fouled conditions for GMF 0.90 and 0.80.

6.1.5 Fouling Effect on Polytropic Efficiency

Dry gas

Figure 6.11 display the polytropic efficiency for both the fouled and clean dry gas tests. A clear reduction in the efficiency can be seen for the fouled case. The reduction is seen to be more pronounced for higher flow rates, which indicates enhanced frictional losses due to fouling. The increase in the frictional losses are primarily linked to increased surface roughness in combination with a flow area reduction increasing the mean flow velocity. In addition to this, the resulting mismatch between the impeller and diffuser section further reduces the efficiency. As a result of the losses being enhanced for increasing flow rates, the BEP is reduced and shifted towards lower flow rates.

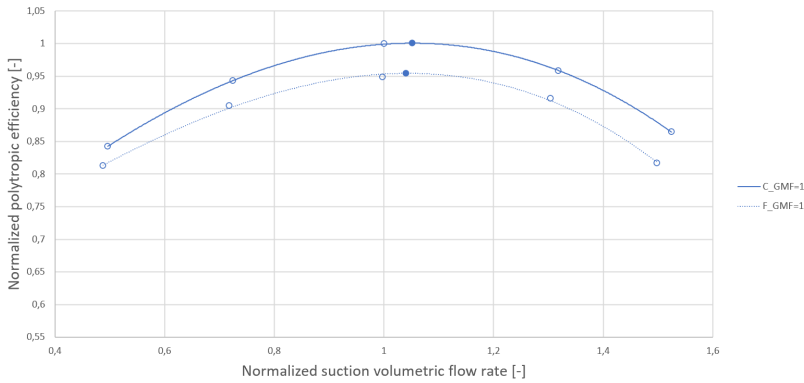


Figure 6.11: Normalized polytropic efficiency curves the for clean and fouled dry gas compression tests.

Wet gas

Figure 6.12 display the polytropic efficiency curves for GMF 0.99 and 0.975 for both clean and fouled conditions. The curve trends are similar to that observed for dry gas where the efficiency curves converge towards low flow rates and diverge towards higher flow rates. It is evident that the fouling of the diffuser section further reduces the efficiency for both GMFs for the tested domain. The tendency of lower GMFs having lower efficiency is still valid for fouled conditions. The location of the BEP is seen to be shifted towards lower flow rates for GMF 0.975 while the location of the BEP with regards to volume flow rate for GMF 0.99 remains the same. The obtained results for polytropic efficiency displayed in Figures 6.11 and 6.12 concur well with the effect described in Section 3.4.

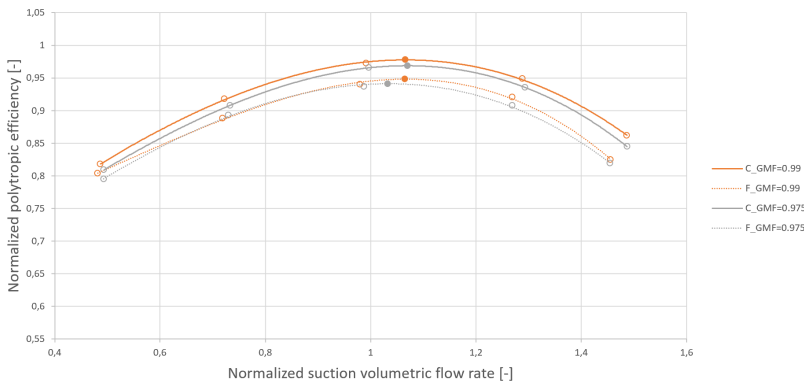


Figure 6.12: Normalized polytropic efficiency curves for clean and fouled conditions for GMF 0.99 and 0.975.

The polytropic efficiency curves for GMF 0.90 and 0.80 can be seen in Figure 6.13. Sim-

ilarly, to both the pressure ratio and polytropic head curves, the efficiency is seen to be increased for the fouled case for both GMF at lower flow compared to the clean base line tests. The effect of fouling causing degradation of the efficiency is however still prominent at higher flow rates. The location of the BEP can be seen further shifted towards lower flow rates for descending GMFs.

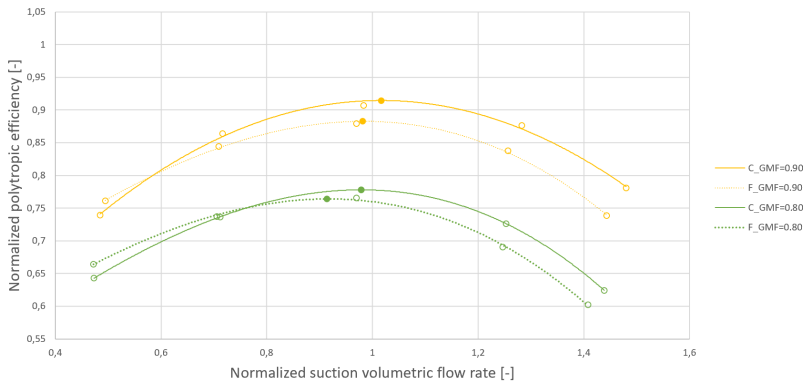


Figure 6.13: Normalized pressure ratio curves for clean and fouled conditions for GMF 0.90 and 0.80.

6.1.6 Deviation in Polytropic Efficiency

The change in polytropic efficiency for the different GMFs when moving from the clean to fouled compressor tests can be seen in Figure 6.14. The curves display the relative reduction in percent for each GMF and is plotted against the normalized suction volumetric flow rate for the fouled tests. The tendency of the reduction in polytropic efficiency being greatest at high flow rates and at its minimum at low flow rates are seen for all tested GMFs. The trends are consistent with the observed trends found in [3]. The slope for the relative change in polytropic efficiency can be seen steeper for lower GMFs. This trend is consistent with the expected results due to the liquid's higher viscosity reacting stronger to the increased roughness than that of the air. The result of the relative reduction being greater for dry gas compared to lower GMFs for almost the entire operational range was however unexpected. The result is comparable with the trend seen in Figure 3.6b. Paulsen and Haugen [3] did however see a significant stronger reduction in the efficiency for lower GMFs compared to dry gas for the roughest fouling tests. In order to verify the obtained results, more testing is needed. A possible explanation for the lower relative change for wet gas compression will be presented in Section 6.2.2.

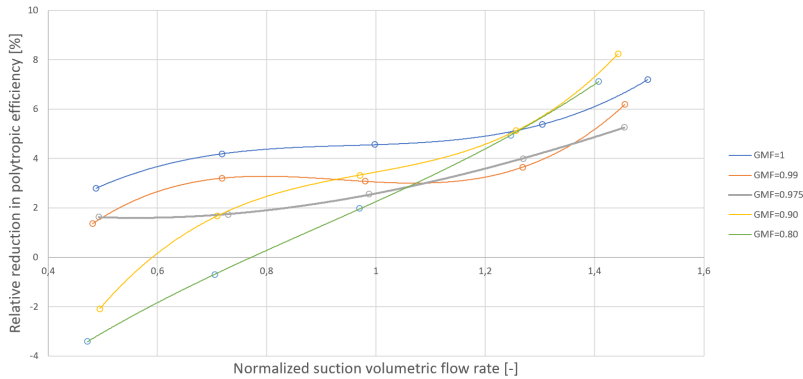


Figure 6.14: The relative reduction in polytropic efficiency when going from clean to fouled scenarios for the tested GMFs.

6.1.7 Fouling Impact on Flow Throughput

From the previous figures it is evident that the maximum flow capacity for the compressor for both dry and wet conditions is further reduced as a consequence of diffuser fouling. The flow reduction can be linked to the increased resistance in the system following the material buildup and increased roughness. The obtained results concur well with that of Haq and Bu-Hazza [30] which observed a clear reduction in mass flow following severe compressor fouling, and Haugen and Paulsen [3] that found fouling of the inducer blades to further reduce the flow rate for both dry and wet gas compression.

6.1.8 Fouling Impact on Surge Margin

From the Figures 6.4, 6.5 and 6.6 there can be observed a twisting of the polytropic head curves due to fouling. The twisting is seen to be greater for reductions in the GMF. The steeper slope towards lower flow rates results in an increase in the head rise to surge for the tested GMFs. The same effect can be seen for the pressure ratio curves seen in Figures 6.8-6.10, resulting in an increased pressure ratio rise to surge. The findings of increased head rise to surge and pressure ratio rise to surge resulting from diffuser fouling, comply well with the results obtained for the inducer section by Paulsen and Haugen [3].

6.2 Coating Experience

Texturized paint had not been utilized as a fouling replica for wet gas compression prior to the conducted experimental campaign. The obtained experimental experience will be beneficial for future testing either further investigating diffuser fouling or utilizing texturized paint.

6.2.1 Wet and Dry Gas Resistance

The fouled diffuser section was inspected prior to initiating the test campaign and between each tested operational point. The strict observation procedure was done in order to quickly spot any onset of wear in the coating and better understanding the mechanism causing the damages to the fouling replica. Special attention was given to the inner radiuses as this was the region thought to be most prone to operational wear.

As the tests were conducted with descending GMFs, the operational load on the coating was gradually increased. As expected, the dry gas compression did not pose any challenges to the coating. There was not observed any damage to the coating for GMF 0.99 and 0.975. For GMF 0.90 there was observed some particles that had detached from the coating, but the damages were still in the top layer. The extent of particle removal was limited and its effect on the diffuser section was deemed negligible. The GMF 0.80 tests showed a slightly increase in the damage to the coating with some spots exposing the red layer (third from the top). Despite piercing through two layers at some spots, the damages to the coating was still minor and the coating was deemed comparable for all tests.

After the test campaign had been conducted and the coating had been inspected, the compressor was operated at GMF 0.80 at maximum flow for 5 hours. The prolonged exposure was done in order to uncover the diffuser zones most susceptible to wear and the severity of the coating damages. The damages inflicted on the coating after the conducted test campaign and 5-hour max load test can be seen next to the initial coating in Figure 6.15. The damaged regions are marked with pink rectangles in both pictures. It can be seen from Figure 6.15a and 6.15b that most of the damages occurs at inner radiuses near the bend of the coating, which is highlighted with a green circle in Figure 4.7. The damages of the inner regions concur well with the expected results and the mass transfer to the hub described in [26]. Despite subjecting the coating to low GMFs for an extended time period, the replica displayed minimal damage or altering of the coating and is therefore recommended for similar testing.

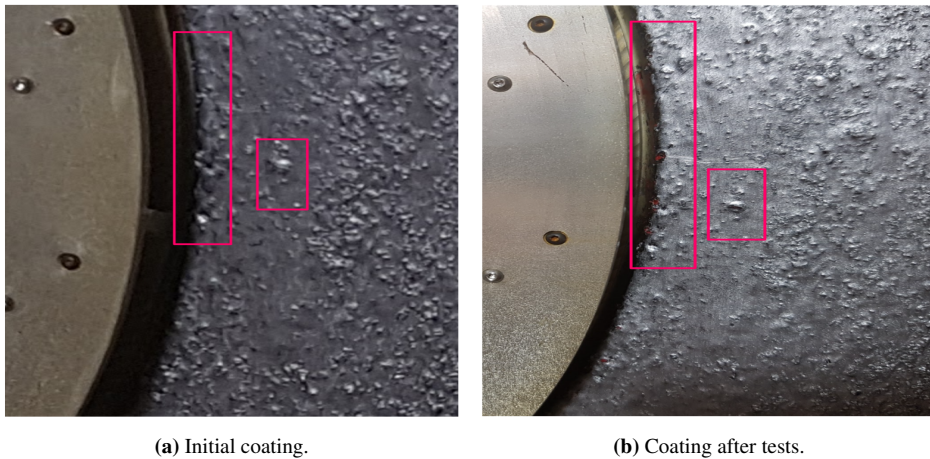


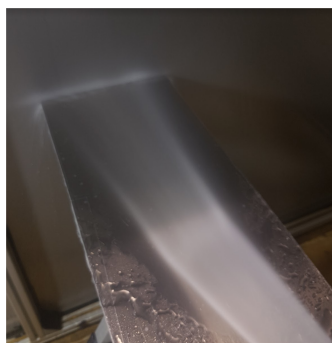
Figure 6.15: State of the coating before and after the conducted experimental campaign and 5 hour maximum load test.

6.2.2 Fouling Influence on Diffuser Flow Pattern

It became evident during the test campaign that the fouled diffuser tests displayed a significantly more chaotic flow pattern than that of the clean tests for wet gas scenarios. It was believed that the difference in flow pattern came as a result of the liquid colliding with the uneven topography of the coating and as a result was redirected away from the surface. To simulate the liquid flow over the clean and fouled diffuser section a flow pattern test was conducted. A power washer stream was directed at both a clean aluminum plate and one plate coated with the texturized paint. The obtained results can be seen in Figures 6.16 and 6.17. From the side view in Figure 6.16a and 6.17a a distinct difference in the liquid flow pattern after impact with the different test plates can be observed. The water is seen extending away from the test plate for the fouled case in contrast to the clean test plate where the water jet is parallel to the surface. In Figure 6.17b it is evident that the described effect of the liquid colliding with the particles and being redirected occurs after impact with the surface. An important observation is that the small water jets extending from the fouled surface does not seem to interact with the coating for the rest of the test plate. This interaction may be a possible explanation to why the relative change in polytropic efficiency was higher for dry gas compared to wet gas compression. The fact that areas of the hub side of the diffuser may experience less water for the fouled scenarios compared to the clean scenarios may counteract the increased roughness effect. In order to validate this, more thorough investigations into fouled diffuser flow regimes for wet and dry gas compression have to be performed.



(a) Side view.



(b) Bird view.

Figure 6.16: Power washer water jet impacting a clean aluminum test plate.



(a) Side view.



(b) Bird view.

Figure 6.17: Power washer water jet impacting a fouled aluminum test plate.

Conclusion and Further Works

An experimental test campaign in addition to a literature review has been conducted to investigate the effect of fouling on the compressor performance with varying GMFs. The effect of fouling in the diffuser section is scarcely documented in literature. Its effect in combination with different GMFs has, to the author's knowledge, never before been documented. The following chapter serves to conclude based on obtained results and discussion as well as present recommendations for further work.

7.1 Conclusion

Fouling of the diffuser section was replicated by applying a total of 11 coats of metallic paint mixed with Plexiglas particles to the hub side of the diffuser. Alternating colors were used for the different coats of paint to easily visualize operational damages inflicted on the coating. Only small damages to the two outermost coats were observed at the inner radiuses after prolonged exposure to high flow rates with low GMFs. This master has thus proven the texturized metallic paint to be a viable option for replicating fouling for wet gas testing.

The experimental results display a clear degradation of the polytropic head and efficiency but an increase in the pressure ratio for descending GMFs at clean conditions. The increase in pressure ratio did however vary little with the liquid content. Fouling was observed to reduce the performance parameters for all GMFs. However, the fouled tests with GMF 0.90 and 0.80 displayed increased performance at low flow rates compared to the clean baseline tests. This observation is thought to be linked to the clean test experiencing surge at an earlier stage than the fouled tests. All fouled tests displayed an increase in head rise to surge and pressure ratio rise to surge compared to the clean conditions, although

more noticeable for lower GMFs. Compared to their respective clean baseline, the fouled maximum efficiency was reduced with a shift in the BEP towards lower flow rates for all tested GMFs. A clear reduction in the maximum throughput was observed for all GMFs at fouled conditions.

Comparing the relative reduction in polytropic head and efficiency when going from clean to fouled conditions clearly display a larger reduction for increasing flow rates. The relative reduction for dry air was observed higher for low to medium flow rates compared to lower GMFs. Results and flow tests indicate that the effect is linked to a reduction in the liquid amount flowing over the hub side at fouled conditions compared to clean conditions. The reduction is a result of extruding particles directing liquid away from the surface.

7.2 Further Works

Based on the acquired knowledge obtained from both literature review and experimental testing, the suggested focus areas for future work are:

- Study the effect of fouling on other compressor components and the resulting impact on the performance characteristics during both wet and dry gas scenarios.
- Investigate the wet gas compression fouling rate with varying liquid content as liquid is documented to both accelerate fouling and clean the compressor internals.
- Investigate the effect different degrees of roughness has on the multiphase boundary layer and the liquid film response when going from clean to fouled conditions.
- Develop new and reliable fouling correction models for centrifugal compressors for both dry and wet gas compression.
- Conduct fouling experiments with different roughness and thickness to obtain information on how the different parameters affect the compressor performance characteristics for changes in GMFs.
- Further investigate the effect of fouling on the compressor operational range, and how it affects the head rise to surge and the onset of surge for different GMFs.

Bibliography

- [1] Equinor. "Starting subsea gas compression – boosting Gullfaks recovery". Available: <https://www.equinor.com/en/news/archive/2015/10/12/12OctGullfakssubseacompression.html>, 2015. (Accessed: 04-06-2020).
- [2] OneSubsea. "Subsea Multiphase Compression System". Available: <https://www.onesubsea.slb.com/subsea-processing-systems/multiphase-wgc-wet-gas-compressor>, 2020. (Accessed: 02-06-2020).
- [3] K. Paulsen and M. P. Haugen. "Fouling Impact on Compressor Performance". Master's thesis, Norwegian University of Science and Technology, 2019.
- [4] B. Bartnes. *Pre-master's project: Compressor Performance Deterioration*. Department of Energy and Process Engineering, NTNU, Trondheim, Norway, 2019.
- [5] S.L. Dixon and C. Hall. *Fluid Mechanics and Thermodynamics of Turbomachinery*. Elsevier Inc, Amsterdam, 7 edition, 2014.
- [6] H. P. Bloch. *A Practical Guide To Compressor Technology*. John Wiley & Sons, Inc, New Jersey, 2 edition, 2006.
- [7] M. Taher and C. Meher-Homji. "Matching of Gas Turbines and Centrifugal Compressors – Oil and Gas Industry Practice ". In *ASME Turbo Expo 2012: Turbine Technical Conference and Exposition*, Copenhagen, Denmark, 2012.
- [8] E. Syverud. "Axial Compressor Performance Deterioration and Recovery through Online Washing". PhD thesis, Norwegian University of Science and Technology, 2007.
- [9] R. H. Aungier. "Mean Streamline Aerodynamic Performance Analysis of Centrifugal Compressors". *Journal of Turbomachinery*, 117(3):360–366, 1995.
- [10] L. E. Bakken. *Compendium: Thermodynamics, Compression and Expansion Processes*. 2017.

-
- [11] ASME PTC-10: *Performance Test Code on Compressors and Exhausters*, 1997.
- [12] ISO 5389: *Turbocompressors — Performance test code*, 2005.
- [13] J. M. Schultz. "The Polytropic Analysis of Centrifugal Compressors". *Journal of Engineering for Power*, 84(1):69–82, 1962.
- [14] Ø. Hundseid, L. E. Bakken, T. G. Grüner, L. Brenne, and T. Bjørge. "Wet Gas Performance of a Single Stage Centrifugal Compressor". In *ASME Turbo Expo 2008: Power for Land, Sea, and Air*, Berlin, Germany, 2008.
- [15] M. Bakken, L. E. Bakken, and T. Bjørge. "Wet Gas Compressor Model Validation". In *ASME Turbo Expo 2019: Turbomachinery Technical Conference and Exposition*, Phoenix, Arizona, USA, 2019.
- [16] T. G. Grüner, L. Brenne, L. E. Bakken, and T. Bjørge. "An Experimental Investigation of Airfoil Performance in Wet Gas Flow". In *ASME Turbo Expo 2008: Power for Land, Sea, and Air*, Berlin, Germany, 2008.
- [17] M. Bakken, T. Bjørge, and L. E. Bakken. "Wet Gas Compressor Operation and Performance". In *ASME 2018 International Mechanical Engineering Congress and Exposition*, Pittsburgh, Pennsylvania, USA, 2018.
- [18] I. S. Diakunchak. "Performance Deterioration in Industrial Gas Turbines". *Journal of Engineering for Gas Turbines and Power*, 114(2):161–168, 1992.
- [19] R. Kurz and K. Brun. "Fouling Mechanisms in Axial Compressors". *Journal of Engineering for Gas Turbines and Power*, 134(3), 2012.
- [20] N. A. Fuchs. *The Mechanics of Aerosols*. Pergamon Press, Oxford, UK, Revised and enlarged edition, 1964.
- [21] D. Bouris, R. Kubo, H. Hirata, and Y. Nakata. "Numerical Comparative Study of Compressor Rotor and Stator Blade Deposition Rates". *Journal of Engineering for Gas Turbines and Power*, 124(3):608–616, 2002.
- [22] A. P. Tarabrin, V. A. Schurovsky, A. I. Bodrov, and J.-P. Stalder. "An Analysis of Axial Compressor Fouling and a Blade Cleaning Method". *Journal of Turbomachinery*, 120(2):256–261, 1998.
- [23] E. Syverud, O. Brekke, and L. E. Bakken. "Axial Compressor Deterioration Caused by Saltwater Ingestion". *Journal of Turbomachinery*, 129(1):119–126, 2007.
- [24] A. P. Tarabrin, V. A. Schurovsky, A. I. Bodrov, and J.-P. Stalder. "Influence of Axial Compressor Fouling on Gas Turbine Unit Performance Based on Different Schemes and With Different Initial Parameters". In *ASME 1998 International Gas Turbine and Aeroengine Congress and Exhibition*, Barcelona, Spain, 1998.
- [25] M. Morini, M. Pinelli, P. R. Spina, and M. Venturini. "Computational Fluid Dynamics Simulation of Fouling on Axial Compressor Stages". *Journal of Engineering for Gas Turbines and Power*, 132(7), 1962.

-
- [26] L. Sun, C. Ma, P. Song, and H. Zhang. "Quantitative computational fluid dynamic analyses of oil droplets deposition on vaneless diffuser walls of a centrifugal compressor". *Energy Science & Engineering*, 8(3):910–921, 2019.
- [27] S. S. Sreedharan and D. K. Tafti. "Composition Dependent Model for the Prediction of Syngas Ash Deposition With Application to a Leading Edge Turbine Vane". In *ASME Turbo Expo 2010: Power for Land, Sea, and Air*, Glasgow, UK, 2010.
- [28] R. Kurz and K. Brun. "Fouling Mechanisms in Axial Compressors". In *Proceedings of ASME Turbo Expo 2011: Turbine Technical Conference and Exposition*, Vancouver, Canada, 2011.
- [29] P. C. Barnard. "Centrifugal compressor fouling- understanding, mitigating and cleaning". In *Compressors and Their Systems: 7th International Conference*, London, UK, 2001.
- [30] I. U. Haq and A. I. Bu-Hazza. "Modeling and Computation of Fouling of a 36MW Multistage Centrifugal Compressor Train Operating in a Cracked Gas Environment". In *ASME Turbo Expo 2001: Power for Land, Sea, and Air*, New Orleans, USA, 2001.
- [31] L. Brenne, T. Bjørge, J. L. Gilarranz, J. M. Koch, and H. F. Miller. "Performance Evaluation Of A Centrifugal Compressor Operating Under Wet Gas Conditions". In *34th Turbomachinery Symposium*, 2005.
- [32] L. Brenne, T. Bjørge, L. E. Bakken, and Ø. Hundseid. "Prospects for Sub Sea Wet Gas Compression". In *ASME Turbo Expo 2008: Power for Land, Sea, and Air*, Berlin, Germany, 2008.
- [33] W. Al-Busaidi and P. Pilidis. "Modelling of the non-reactive deposits impact on centrifugal compressor aerothermo dynamic performance". *Engineering Failure Analysis*, 60:57–85, 2016.
- [34] Y. Ju and C. Zhang. "Robust design optimization method for centrifugal impellers under surface roughness uncertainties due to blade fouling". *Chinese Journal of Mechanical Engineering*, 29(2):301–314, 2016.
- [35] N. A. Cumpsty. *Compressor Aerodynamics*. Longman Scientific & Technical, Essex, UK, 1989.
- [36] R. A. Strub, L. Bonciani, C. J. Borer, M. V. Casey, S. L. Cole, B. B. Cook, J. Kotzur, H. Simon, and M. A. Strite. "Influence of the Reynolds Number on the Performance of Centrifugal Compressors". *Journal of Turbomachinery*, 109(4):541–544, 1987.
- [37] E. Syverud and L. E. Bakken. "The Impact of Surface Roughness on Axial Compressor Performance Deterioration". In *ASME Turbo Expo 2006: Power for Land, Sea, and Air*, Barcelona, Spain, 2008.
- [38] L. Scarbolo, E. Belardini, E. F. Bellobuono, D. T. Rubino, and L. Tapinassi. "Reynolds Correction in Centrifugal Compressors: Theory and Experimental Validation of a Revised Correlation". In *ASME Turbo Expo 2016: Turbomachinery Technical Conference and Exposition*, Seoul, South Korea, 2016.
-

-
- [39] K. L. Suder, R. V. Chima, A. J. Strazisar, and W. B. Roberts. "The Effect of Adding Roughness and Thickness to a Transonic Axial Compressor Rotor". *Journal of Turbomachinery*, 117(4):491–505, 1995.
- [40] G. Jombo, J. Pecinka, S. Sampath, and D. Mba. "Influence of Fouling on Compressor Dynamics: Experimental and Modeling Approach". *Journal of Engineering for Gas Turbines and Power*, 140(3), 2018.
- [41] Hammerite - Direct to Rust Metal Paint Hammered. Available: <https://www.hammerite.no/product/hamme-effect/>.
- [42] Quick Bengalack Universal. Available: <https://www.quickbengalack.no/produkter/universal>.
- [43] M. Bakken and T. Bjørge. "An Experimental Investigation on Hysteresis in a Wet Gas Compressor". In *ASME 2017 Gas Turbine India Conference*, Bangalore, India, 2017.
- [44] T. G. Grüner and L. E. Bakken. "Wet Gas Impeller Test Facility". In *ASME Turbo Expo 2010: Power for Land, Sea, and Air*, Glasgow, UK, 2010.
- [45] ISO 5167-2: *Measurement of fluid flow by means of pressure differential devices inserted in circular cross-section conduits running full — Part 2: Orifice plates*, 2003.
- [46] BETE. "NF Nozzles: High Impact Flat Fan and Standard Fan Nozzles". Available: <https://www.bete.com/products/nf>, 2020. (Accessed: 21-06-2020).
- [47] L. E. Bakken and Ø. Hundseid. "Integrated Wet Gas Compressor Test Facility". In *ASME Turbo Expo 2015: Turbine Technical Conference and Exposition*, Montreal, Quebec, Canada, 2015.
- [48] S. Madsen and L. E. Bakken. "Gas Turbine Fouling Offshore: Correction Methodology Compressor Efficiency". In *ASME Turbo Expo 2017: Turbomachinery Technical Conference and Exposition*, Charlotte, North Carolina, USA, 2017.
- [49] M. Svensson. "Wet Gas Compression: Effect of a liquid phase on radial compressor performance". Master's thesis, Lund University, 2014.
- [50] Hysys AspenTech. "Simulation Basis", 2008. Available: <https://sites.ualberta.ca/CMENG/che312/F06ChE416/HysysDocs/AspenHYSYSsimulationBasis.pdf> (Accessed: 30-05-2020).

Schultz Method

Schultz [13] aimed to derive the real-gas equations of polytropic analysis and display their application towards centrifugal compressor design and testing. Schultz accomplished this by introducing two new compressibility factors, X and Y , related to the isentropic and isothermal compressibility, respectively. These two compression functions would accompany the already utilized compressibility factor Z . In the same way as Z , these compressibility functions can be generalized and plotted for different gases in corresponding states and are given by:

$$X = \frac{T}{v} \left(\frac{\partial v}{\partial T} \right)_p - 1 \quad (\text{A.1})$$

$$Y = -\frac{p}{v} \left(\frac{\partial v}{\partial p} \right)_T \quad (\text{A.2})$$

The averaged compressibility functions over the compressor section are defined as:

$$X = \frac{X_1 + 2X_{mid} + X_2}{4} \quad (\text{A.3})$$

$$Y = \frac{Y_1 + 2Y_{mid} + Y_2}{4} \quad (\text{A.4})$$

By implementing the compressibility functions X and Y Schultz was able to predict the change in the polytropic volume exponent, n_v , and the polytropic temperature exponent, n_T , along the real gas compression path.

$$n_v = \frac{1 + X}{Y \left[\frac{1}{k} \left(\frac{1}{\eta_p} + X \right) - \left(\frac{1}{\eta_p} - 1 \right) \right]} \quad (\text{A.5})$$

$$\frac{n_T - 1}{n_T} = \frac{k - 1}{k} \frac{\left(\frac{1}{\eta_p} + X \right) Y}{(1 + X)^2} \quad (\text{A.6})$$

As n_v and n_T varies along the compression path, an analytical solution of the polytropic head is impossible. At the time Schultz introduced his research, numerical computational tools were in their cradle. The polytropic exponent was thus assumed constant through the compression process which can be seen in Equation A.7. In order to correct for this assumption, Schultz introduced a head correction factor, f , to be added to the equation.

$$H_p = \int_1^2 v dp \approx \frac{n_v}{n_v - 1} (p_2 v_2 - p_1 v_1) \quad (\text{A.7})$$

The head correction factor is assumed equal for isentropic and polytropic analysis and is given by:

$$f = f_p = f_s = \frac{h_{2s} - h_1}{\frac{\kappa_v}{\kappa_v - 1} (p_2 v_{2s} - p_1 v_1)} \quad (\text{A.8})$$

Based on this the polytropic head can be computed by Equation A.9 or A.10.

$$H_p = \int_1^2 v dp \approx f \frac{n_v}{n_v - 1} (p_2 v_2 - p_1 v_1) \quad (\text{A.9})$$

$$H_p = \int_1^2 v dp \approx f \frac{n_v}{n_v - 1} \frac{Z_1 R_0 T_1}{MW} \left[\left(\frac{p_2}{p_1} \right)^{\frac{n_v - 1}{n_v}} - 1 \right] \quad (\text{A.10})$$

When the polytropic head and total head is known, the polytropic efficiency can be computed by:

$$\eta_p = \frac{dh_p}{dh} = \frac{v dp}{dh} = \frac{H_p}{H} \quad (\text{A.11})$$

Appendix B

HYSYS Model

The steady state HYSYS model depicted in Figure B.1 was used to calculate the polytropic head and efficiency for the different compressor tests. Soave-Redlich-Kwong was chosen as the equation of state due to its comparable results with the NTNU wet gas compressor test facility. An in-depth coverage of the simulation basis can be found in [50].

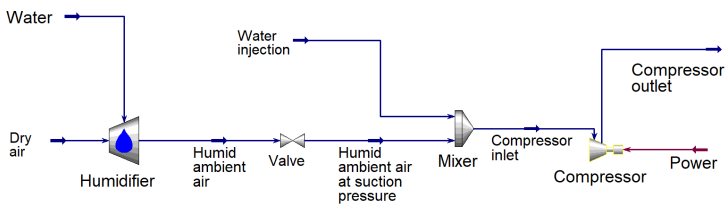


Figure B.1: HYSYS steady state model used for polytropic head and efficiency calculations.

The dry air stream is specified with the measured ambient air parameters where the relative humidity is accounted for by the *humidifier*. The stream is then sent through a *valve* to simulate the suction pressure of the compressor. The water injection module is simulated by the *mixer*. The *water injection* stream, with its specified mass flow rate and temperature, is mixed with the *humid ambient air at suction pressure*. The result is a homogeneous mix with an equilibrium temperature that serves as the inlet temperature for the wet gas compression tests. The liquid mass flow of the *water injection* was set to a value of $1\text{E-}9$ kg/h for dry gas simulations. Setting the water stream to zero result in enthalpy discontinuity between the temperature readings at ambient and inlet conditions. The small water injection corrects for this without affecting the other parameters or the mass flow which for dry air will be in the range of 2.3-6,7E3 kg/h.



The *compressor inlet* stream is connected to the *compressor* where the rotational speed is defined in addition to selecting the compressor as centrifugal. HYSYS signals a warning to the user that liquid is entering the compressor by displaying a yellow outline of the compressor indicating that it is operating outside its intended use. The outlet pressure is specified in the *compressor outlet* stream. Due to unreliable temperature readings in multiphase flow, the compressor power requirement given by the *power* stream, is utilized instead. For dry gas scenarios both outlet temperature and compressor power can be utilized.

The calculated polytropic heads and efficiencies for the different tests were gathered to form the compressor curves given in Chapter 6. Hundseid et al. [14] states that a direct integration of the polytropic performance along the compression path increases the accuracy for wet gas compression compared to Schultz method. The polytropic analysis in HYSYS has thus been carried out by the “reference” polytropic method which performs piecewise integration along the actual compression path. The difference between Shultz and the reference method are typically low and particularly for low pressure settings. HYSYS does not utilize the compressibility factors X and Y given in Appendix A – Schultz Method but rather equates the polytropic properties by obtaining the exit specific volume, v_2 , through the chosen equation of state. The obtained results from the two different polytropic methods will thus be almost equal.

Appendix C

Risk Matrix

The risk matrix of the experimental campaign for the current master's thesis and the corresponding consequence and likelihood explanations are presented in the following pages.

NTNU	Risk assessment			Prepared by	Number	Date	
				HSE section	HMSRV/2603E	04.02.2011	
HSE/KS				Approved by		Replaces	
				The Rector		01.12.2006	

Unit: Department of Energy and Process Engineering

Date: **January 2020**


Line manager: Terese Lovås

Participants in the identification process (including their function):

Student: Bendik Barthes Lab engineer: Erik Langørgen


Short description of the main activity/main process: Wet and dry gas compression performance deterioration from fouling, Master project

Is the project work purely theoretical? NO

Signatures: Responsible supervisor: 

Student: 

Activity from the identification process form	Potential undesirable incident/strain	Likelihood (1-5)	Consequence:		Risk Value (human)	Comments/status Suggested measures
			Human (A-E)	Environment (A-E)		
Application of texturized paint.	Inhaling potential harmful fumes.	1	D	A	D1	Using painting mask and fan to increase air circulation.
Dry and wet gas experiments (with or without fouling).	Inflicted hearing damage.	1	D	A	D1	Use hearing protection at all times and minimize prolonged exposure.
Dry and wet gas experiments (with or without fouling).	Plexiglas window breaking or shattering.	1	D	A	D1	Use protective glasses and follow laboratory guidelines.
Dry and wet gas experiments (with or without fouling).	Mechanical failure due to rapid load increase.	1	D	A	D1	Slowly increase load, until reaching desired set point. Use operating guidelines.
Dry and wet gas experiments (with or without fouling).	Mechanical wear/stress causing parts entering the impeller and risking getting flung out.	1	D	A	D1	Visual inspection and routinely maintenance.
Fouling experiment applied texturized paint.	Tear-off during testing, causing damages/scratches to the compressor/downstream equipment and piping.	3	A	A	A3	Visual inspection of the coating before, during and after tests.
Removal of texturized paint	Damages inflicted on diffuser section.	1	A	A	A1	Use Plexiglas scrape.
Removal of texturized paint	Skin contact with paint remover.	1	C	A	C1	Use protective gloves and long sleeve shirt.

NTNU			
HSE/IKS			
Risk assessment			
Prepared by	Number	Date	
HSE section	HMSRV/2603E	04.02.2011	
Approved by		Replaces	
The Redtor		01.12.2006	

Potential undesirable incident/strain
Identify possible incidents and conditions that may lead to situations that pose a hazard to people, the environment and any materiel/equipment involved.

Criteria for the assessment of likelihood and consequence in relation to fieldwork

Each activity is assessed according to a worst-case scenario. Likelihood and consequence are to be assessed separately for each potential undesirable incident. Before starting on the quantification, the participants should agree what they understand by the assessment criteria:

Likelihood	Low 2	Medium 3	High 4	Very high 5
Minimal 1	Once every 10 years or less	Once a year or less	Once a month or less	Once a week

Consequence Grading	Human	Environment	Financial/material
E Very critical	May produce fatality/ies	Very prolonged, non-reversible damage	Shutdown of work > 1 year.
D Critical	Permanent injury, may produce serious health damage/sickness	Prolonged damage. Long recovery time.	Shutdown of work 0.5-1 year.
C Dangerous	Serious personal injury	Minor damage. Long recovery time	Shutdown of work < 1 month
B Relatively safe	Injury that requires medical treatment	Minor damage. Short recovery time	Shutdown of work < 1week
A Safe	Injury that requires first aid	Insignificant damage. Short recovery time	Shutdown of work < 1day


The unit makes its own decision as to whether opting to fill in or not consequences for economy/material, for example if the unit is going to use particularly valuable equipment. It is up to the individual unit to choose the assessment criteria for this column.

Risk = Likelihood x Consequence

Please calculate the risk value for "Human", "Environment" and, if chosen, "Economy/material", separately.

About the column "Comments/status, suggested preventative and corrective measures":

Measures can impact on both likelihood and consequences. Prioritise measures that can prevent the incident from occurring; in other words, likelihood-reducing measures are to be prioritised above greater emergency preparedness, i.e. consequence-reducing measures.

NTNU		prepared by		Number		Date	
 HSE/KS		HSE Section		HMSRV2604		8 March 2010	
		approved by		Page		Replaces	
		Rector		4 of 4		9 February 2010	
Risk matrix							



MATRIX FOR RISK ASSESSMENTS at NTNU

		CONSEQUENCE					LIKELIHOOD				
		Extremely serious	E1	E2	E3	E4	E5	Very low	Low	Medium	High
Serious		D1	D2	D3	D4	D5					
Moderate		C1	C2	C3	C4	C5					
Minor		B1	B2	B3	B4	B5					
Not significant		A1	A2	A3	A4	A5					

Principle for acceptance criteria. Explanation of the colours used in the risk matrix.

Colour	Description
Red	Unacceptable risk. Measures must be taken to reduce the risk.
Yellow	Assessment range. Measures must be considered.
Green	Acceptable risk. Measures can be considered based on other considerations.

